Aerodynamic Analysis of Variable Geometry Raked Wingtips for Mid-Range Transonic Transport Aircraft

David J. Jingeleski

Thesis submitted to the faculty of the Virginia Polytechnic Institute and State University
in partial fulfillment of the requirements for the degree of

Master of Science
In
Aerospace Engineering

Joseph A. Schetz, Chair
Rakesh K. Kapania
Craig A. Woolsey

December 6, 2012
Blacksburg, VA

Keywords: variable geometry wingtip, roll control, gust alleviation

Aerodynamic Analysis of Variable Geometry Raked Wingtips for Mid-Range Transonic Transport Aircraft

David J. Jingeleski

ABSTRACT

Previous applications have shown that a wingtip treatment on a commercial airliner will reduce drag and increase fuel efficiency and the most common types of treatment are blended winglets and raked wingtips. With Boeing currently investigating novel designs for its next generation of airliners, a variable geometry raked wingtip novel control effector (VGRWT/NCE) was studied to determine the aerodynamic performance benefits over an untreated wingtip. The Boeing SUGAR design employing a truss-braced wing was selected as the baseline. Vortex lattice method (VLM) and computational fluid dynamics (CFD) software was implemented to analyze the aerodynamic performance of such a configuration applied to a next-generation, transonic, mid-range transport aircraft. Several models were created to simulate various sweep positions for the VGRWT/NCE tip, as well as a baseline model with an untreated wingtip. The majority of investigation was conducted using the VLM software, with CFD used largely as a validation of the VLM analysis. The VGRWT/NCE tip was shown to increase the lift of the wing while also decreasing the drag. As expected, the unswept VGRWT/NCE tip increases the amount of lift available over the untreated wingtip, which will be very beneficial for take-off and landing. Similarly, the swept VGRWT/NCE tip reduced the drag of the wing during cruise compared to the unmodified tip, which will favorably impact the fuel efficiency of the aircraft. Also, the swept VGRWT/NCE tip showed an increase in moment compared to the unmodified wingtip, implying an increase in stability, as well providing an avenue for roll control and gust alleviation for flexible wings. CFD analysis validated VLM as a useful low fidelity tool that yielded quite accurate results. The main results of this study are tabulated “deltas” in the forces and moments on the VGRWT/NCE tip as a function of sweep angle and aileron deflection compared to the baseline wing. A side study of the effects of the joint between the main wing and the movable tip showed that the drag impact can be kept small by careful design.

Acknowledgements

First, I would like to thank my advisor, Dr. Schetz, for his constant advice and support. Without his expertise and guidance this project would not have been possible. I would also like to thank my other committee members, Dr. Kapania and Dr. Woolsey, for their collaboration and assistance. Due to the collaborative effort between Boeing and Virginia Tech, I would be also like to thank Ed White, principal investigator of the NCE project, for his support and direction during this endeavor. This project was supported by funds from NASA and I am grateful for their contribution.

On a personal note, I would like to thank my parents and sister for their constant encouragement, support, and reassurance during this adventure. Without this I never could have come this far. I would also like to thank Brittany Rich for her continuous encouragement, optimism, and for understanding why I could not come home every weekend. Finally, I would also like to thank my fellow graduate students for their support and encouragement: Donny Brooks, John Coggin, Ryan Montero, David Owens, Mark Palframan, and Kevin Sheets.

Table of Contents

List of Figures

List of Tables

List of Equations

Nomenclature

AR	Aspect ratio
c	chord
C_D	Drag coefficient
$C_{D_{step}}$	Drag coefficient of step
$C_{D_{tip}}$	Drag coefficient of wingtip only
c_D	Independent drag coefficient
C_{D0}	Zero lift drag coefficient
C_L	Lift coefficient
$C_{M_{c/4}}$	Moment coefficient about quarter chord
e	Oswald efficiency factor
h	Step height
S_{tip}	Area of wingtip
x	Distance from leading edge to step
β	Step incidence angle
ΔC_{Force}	Change in resultant force
ΔC_{Moment}	Change in moment
Λ_{LE}	Leading edge sweep angle

Chapter 1: Introduction

The aerospace community is constantly investigating new and exciting concepts for the improved performance of transport aircraft. To this end, NASA commissioned a research project looking into the next generation of passenger aircraft, and Boeing developed several subsonic and supersonic concepts designed to meet NASA's goals. The subsonic ultra-green aircraft research (SUGAR) produced many concepts, from conventional low- wing configurations, to high-wing, truss-braced configurations, to blended-wing-body arrangements [1]. Of the conventional designs, the truss-braced wing (TBW) concept is particularly interesting for medium-range aircraft due to the fact that it is not entirely dependent on ambiguous "future technologies". The concept is also easily scalable to various aircraft sizes. Using current technology, tangible gains in fuel efficiency, range and payload, along with a reduction of aircraft weight, are possible simply by incorporating a strut and jury wing design [2]. With the baseline SUGAR research completed by Boeing, methods of further improving the designs are underway. A relatively straightforward way to improve aerodynamics and fuel efficiency is to include a wingtip treatment, such as a winglet or raked tip.

In the pursuit of fuel efficiency and drag reduction, the current crop of Boeing and Airbus airliners incorporates some type of wingtip treatment. One common type of treatment is vertically blended winglets, evident on the Boeing 737 and 747. The main benefits of blended winglets are to increase range and payload, while decreasing fuel usage. This is accomplished by decreasing the induced drag of the wing. The winglet decreases induced drag by increasing the velocity of the flow over the tip, which produces additional lift and improves the wing lift distribution. The end result of this procedure is a reduction a trailing vortex strength, which improves efficiency [3].

Another common type of treatment is the horizontally raked wingtip, found on the Boeing 767 and 787. Generally, a raked tip necessitates structural enhancements due to the increase in span and is, therefore, commonly only applied to new designs. The winglet however, does not suffer from this problem, thus it is more easily adapted to existing designs, as was carried out with the Boeing 737 and 747. Ideally, the wing span should be maximized during take-off and landing in order to produce the most lift during these critical flight regimes. However, in order to decrease drag during transonic cruise conditions, the wing should be swept and span reduced in order to avoid unnecessary drag caused by locally supersonic flow over the wing. The raked wingtip represents a compromise between these two extremes by having the tip swept at an angle such that improvements are made in all flight areas [4]. However, in order to gain the maximum performance increase over the entire flight envelope, the tip should swing in response to current flight conditions. A variable sweep wing is not a new concept, and has been incorporated on military aircraft in the past.

Messerschmitt first studied variable sweep wings during World War II, though the concept was unfinished before the war's conclusion. Experimental aircraft were built and flown in the United States in the post-war period, however results were mixed [5]. The first production swing wing aircraft was the F-111 Aardvark, however the most famous is arguably the F-14 Tomcat [6]. The F-14's mission represents all of the classic design conditions for a swing wing. The wing extends for carrier take-off and landing, when lift and maneuverability are paramount, and retracts during transonic cruise to decrease drag and allow a higher cruise Mach number [6]. The same performance gains are obtainable with a variable sweep raked wingtip, though to a lesser degree. A study of the aerodynamics of a variable geometry raked wingtip (VGRWT) is of interest due to the possible improved aerodynamics of the wing system. Additionally, an

important potential of a variable sweep wingtip is as a novel control effector (NCE), which utilizes the generation of torque on a flexible wing as a means of roll control, as well as gust and/or flutter alleviation. Thus, we will refer to this system as a VGRWT/NCE. Therefore, due to the possible aforementioned performance gains, a variable sweep raked wingtip was selected as the tip treatment for the Boeing SUGAR design employing a truss-braced wing to be studied by a team including Boeing, Virginia Tech, and NextGen Aeronautics.

Boeing designed the VGRWT/NCE to replace the conventional tip on the current SUGAR design. The tip is designed to be of the same area, however the span would be increased. This results in the unswept tip displaying nearly the same aerodynamic properties as the conventional tip. Furthermore, it was nominally decided to set the maximum sweep angle to 50°. Also the unswept state would have a sweep equal to the main wing structure, approximately 15°. Though it is possible to sweep the tip forward, this was not investigated due to the structural considerations required to resist divergence. Finally, since the tip is to be swept during cruise and the majority of flight time is spent at this stage, the fully-swept case was designed to be the default state of the tip.

The aerodynamic performance of the tip was analyzed using an inviscid vortex lattice method (VLM) Matlab code, as well as a computational fluid dynamics (CFD) program. The aim of this analysis is to produce the changes ("deltas") in force and moment on the tip compared to the baseline SUGAR wingtip over a range of tip sweep and aileron deflection angle. Using these tools, it will be shown that the VGRWT outperforms the unaffected tip, in terms of lift and moment produced.

Chapter 2: Methods and Models

2.1 Vortex Lattice Method

The vortex lattice method was selected as the main tool for assessing aerodynamic performance changes on the wingtip, because it allows for comprehensive studies over a wide parameter space due to its speed and robustness [7]. *Tornado* is a VLM code written for Matlab, initially developed as a Master's thesis in Sweden [8]. It provides a way to examine many different aircraft shapes in a relatively short amount of time. With the excellent correlation with data provided by Cessna, *Tornado* provides a flexible and well-validated low fidelity aerodynamic analysis tool [8]. The code computes the vortical strength in the usual way, however a notable difference occurs in the handling of the freestream following the downwash. In *Tornado*, the wake vortex is realigned with the freestream at a point in the downwash where the aerodynamic influence of the vortex line is negligible. This method allows *Tornado* to incorporate wing twist and aileron deflections into the design. Therefore, given *Tornado's* large included airfoil database, as well as the ability to import custom airfoils, the range of wing profiles that can be created is very wide [8,9]. This includes the ability to analyze more than one aerodynamic surface, which proved very useful considering that the baseline SUGAR configuration incorporates a strut and jury. *Tornado* also provides several options for panel distribution, and prior work has shown that the spanwise half-cosine method gives the least error in the prediction of the aerodynamic center [10]. Therefore, that was chosen for all models here. However, VLM codes do have some notable drawbacks.

Though *Tornado* is a useful tool for low-fidelity aerodynamic analysis, it lacks viscous modes. This is a shortcoming of all VLM codes and can be mitigated through the use of empirical corrections. *Tornado* also has no method to predict stall, leading to inaccuracy at high

angles of attack. This is not a problem for this research, since all analysis is conducted at cruise conditions, which implies very small angles of attack. VLM codes also do not typically have compressibility corrections and indeed early versions of *Tornado* did not. However, current versions of *Tornado* do include the Prandtl-Glauert correction, and this has proven to be quite effective at modeling compressibility, with results comparing very well to experimental data [11]. Finally, a common complaint regarding VLM codes is perceived inaccuracy in the calculation of the pitching moment. However, careful placement of the moment reference point, in this case taken to be the quarter chord of the root, can somewhat lessen this inaccuracy.

2.2 Computational Fluid Dynamics

As computing power has increased, CFD has become a powerful tool for aerodynamic analysis. The program chosen here to do the analysis was *ANSYS Fluent*, due to previous research experience with the program and a largely automated configuration, especially regarding grid generation. *Fluent* proved relatively easy to use, once a reasonable amount of time had been spent learning its intricacies. Similar to *Tornado*, *Fluent* allows for nearly limitless model types, assuming they can be adequately reproduced with a CAD program, and proper mesh generation is performed. The CAD program used for this analysis was *Fluent's* built-in studio, DesignModeler. Similarly, the mesher used was *Fluent's* built-in mesh generator, which automatically generated the mesh based on a set of specifications, such as element size and shape, curvature angle, and grid type. This analysis was started with a relatively simple mesh, then adaptive gridding was conducted to demonstrate grid independence. Although *Fluent* ran quickly by CFD standards, this research required many iterations and geometries, therefore the time penalty became untenable. Consequently, this research uses *Fluent* as a collaborative tool

with *Tornado*. The *Fluent* solutions were run inviscid and compressible, and they were used primarily to validate the *Tornado* results for a few interesting cases, but the bulk of the analysis was left to the considerably faster VLM code. This analysis strategy is deemed appropriate, since the goal is to determine the "deltas" between the tip of the baseline SUGAR wing and VGRWT/NCE wingtip.

2.3 Design of VGRWT/NCE Tip

In order to incorporate the VGRWT/NCE tip, the baseline SUGAR wing design was modified. After several concepts and iterations with Boeing engineers, it was decided that the location of the pivot point of the VGRWT/NCE tip should be at the rear spar of the wing, approximately 60% of the chord. This design necessitates tucking a portion of the leading edge into the main wing when the tip is unswept. When the VGRWT/NCE tip transitions to the fully swept position, this section will extend, while a portion of the trailing edge moves into the main wing. An early sketch of this design is shown as Figure 1. Note that although the pivot point is incorrect in this sketch, the concept for the pivot mechanism is the same.

The span of the VGRWT/NCE tip was designed to adhere to the "2/3 rule". This rule of thumb states that the span of the tip will only increase the span of the wing by 1/3 of the length of the span of the tip. The fully-swept span of the VGRWT/NCE tip was set to be 120 inches, which necessitates that the VGRWT/NCE tip will begin at the 939 inch span station of the SUGAR wing, for a net gain of 40 inches of span according to the 2/3 rule. However, this does not include the span increase due to the deployment of the sweep mechanism. This deployment brings the total tip span to approximately 145 inches. A sketch of the fully-swept VGRWT/NCE

tip geometry is shown as Figure 2. From this point, the geometry of the VGRWT/NCE tip determined that the unswept tip must have a span of 193 inches.

Planform data for the baseline SUGAR TBW main wing was provided by Boeing and is the result of their multidisciplinary design optimization (MDO) analysis. The wing twist per span and wing thickness per span is reproduced as Figure 3. Since the VGRWT/NCE tip increases the span, the thickness and twist profiles were adapted to reflect this increase. Also, the areas of constant twist and thickness, at approximately 0.9 span, reflect where the NCE tip joins the main SUGAR planform. Wing twist and thickness was kept constant in order to facilitate the implementation of the swing mechanism.

In order to accurately compare VGRWT/NCE tip performance with the baseline SUGAR tip, the boundary for the baseline SUGAR tip was extended inwards to the approximately 880 in spanstation. This allows the baseline SUGAR tip to be of comparable area to the VGRWT/NCE tip and to incorporate an equal size aileron, as will be discussed in Section 2.5. As will be seen in Chapter 3, this proves correct as the baseline SUGAR tip provides nearly identical performance to the unswept VGRWT/NCE tip, as desired.

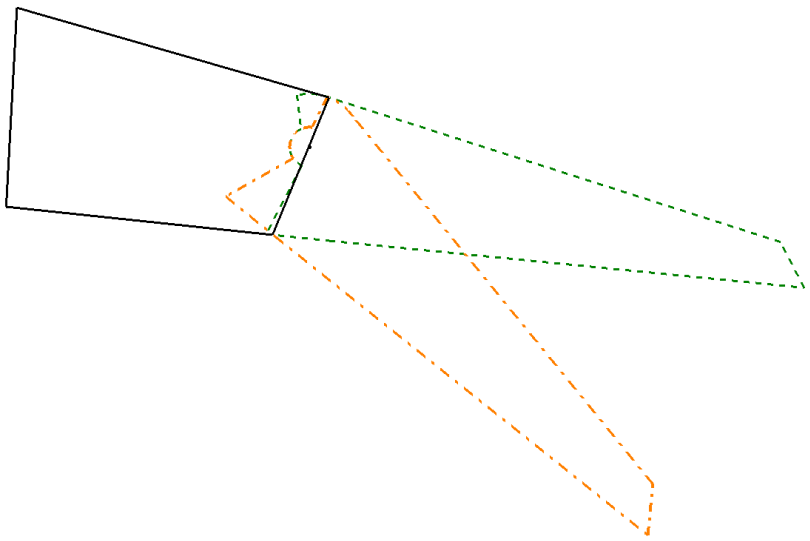

Figure 1 – Early Sketch of VGRWT/NCE Tip Pivot Concept

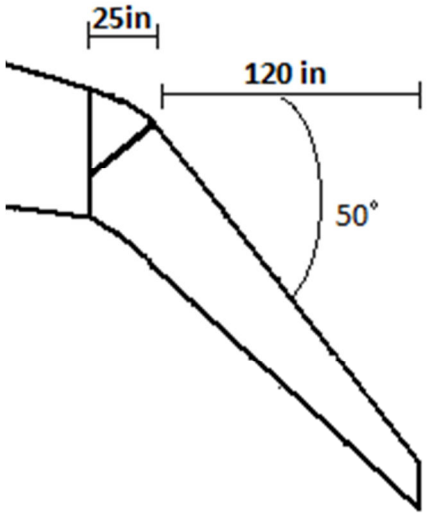

Figure 2 – Geometry Sketch of Fully-Swept VGRWT/NCE Tip

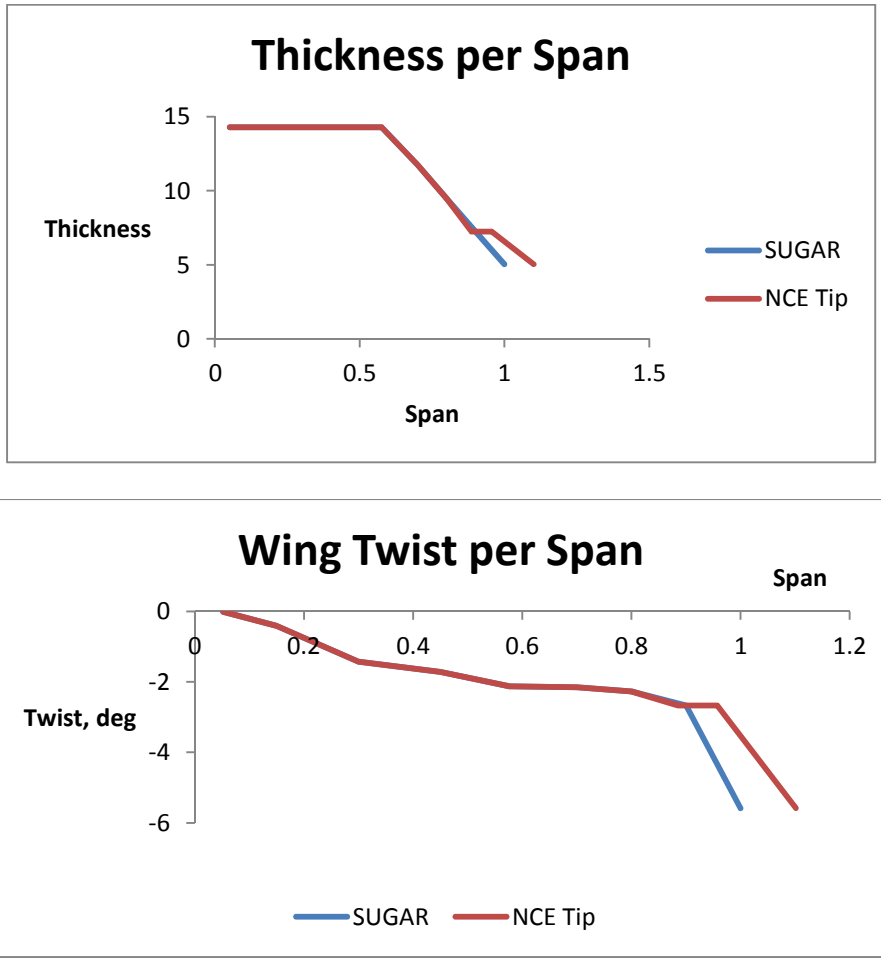

Figure 3 – Wing Thickness and Twist per Span for SUGAR and VGRWT/NCE Tip

2.4 Clean Wing Models

Preliminary analysis was first conducted using the baseline SUGAR TBW main wing, but without the strut, jury or ailerons. The publically available Boeing Aircraft Company J (BACJ) airfoil was chosen as a suitable representative of the supercritical airfoils found on many current airliners, and Figure 4 depicts its shape [12]. All calculations were carried out at cruise conditions, specifically Mach 0.7 and 44,000 ft altitude.

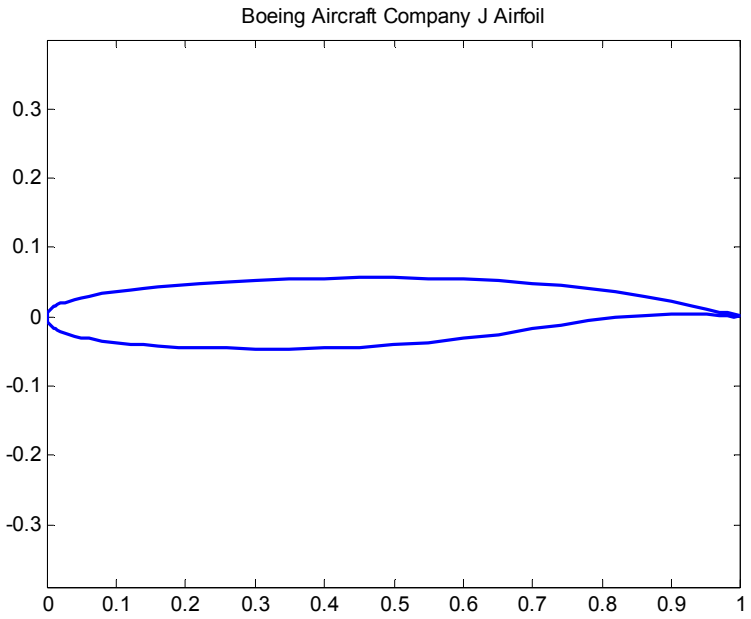

Figure 4 – Boeing Aircraft Company J airfoil [12]

2.4.1 Tornado Models

Models of the clean wing were constructed in *Tornado* for the baseline SUGAR main wing planform, unswept-tip case, and fully-swept VGRWT/NCE tip case. *Tornado* does not allow for geometry to be rotated to create a new model. Therefore, each model must be made independently of others. Further, the boundary of each wing section must be streamwise. In actuality, the boundary between the main wing and the NCE tip is normal to the leading edge,

however, given the aforementioned limitation that section boundaries must be streamwise, this is impossible to model in *Tornado*. The resulting very slight reduction in tip area would not meaningfully influence the results. The baseline SUGAR model constructed in *Tornado* shows excellent convergence with the data provided by Boeing, as shown in Table 1. Table 2 compares all of the wing models constructed in *Tornado*, and shows good agreement between wing areas for the unswept and swept cases, as desired. Each model consists of approximately 300 panels, with panel density increasing towards the tip. Figure 5 shows the *Tornado* clean wing models used for preliminary analysis. Note that only the half span is shown for clarity.

Also, in a real application the design of the wingtip necessitates a small step at the joint of the main wing and the VGRWT/NCE tip. Due to the constraints of *Tornado*, this step was not incorporated into any *Tornado* models. A drag estimation method developed to deal with the influence of the step will be discussed in Section 3.3.

Table 1 – Comparison of SUGAR Main Wing Planforms

	Baseline SUGAR Planform	***Tornado* Model**
Area (ft^2)	1477.11	1476.69
Span (in)	2039.3	2039.29
Aspect Ratio	19.55	19.56
Mean Aerodynamic Chord (in)	110.286	110.256

Table 2 – Comparison of *Tornado* Wing Models

	Baseline Main SUGAR Wing	**SUGAR Main Wing with Unswept VGRWT/NCE Tip**	**SUGAR Main Wing with Fully-Swept VGRWT/NCE Tip**
Area (ft^2)	1476.69	1512.39	1511.91
Span (in)	2039.29	2265.79	2172.87
Aspect Ratio	19.56	23.54	21.69
Mean Aerodynamic Chord (in)	110.26	108.15	108.73

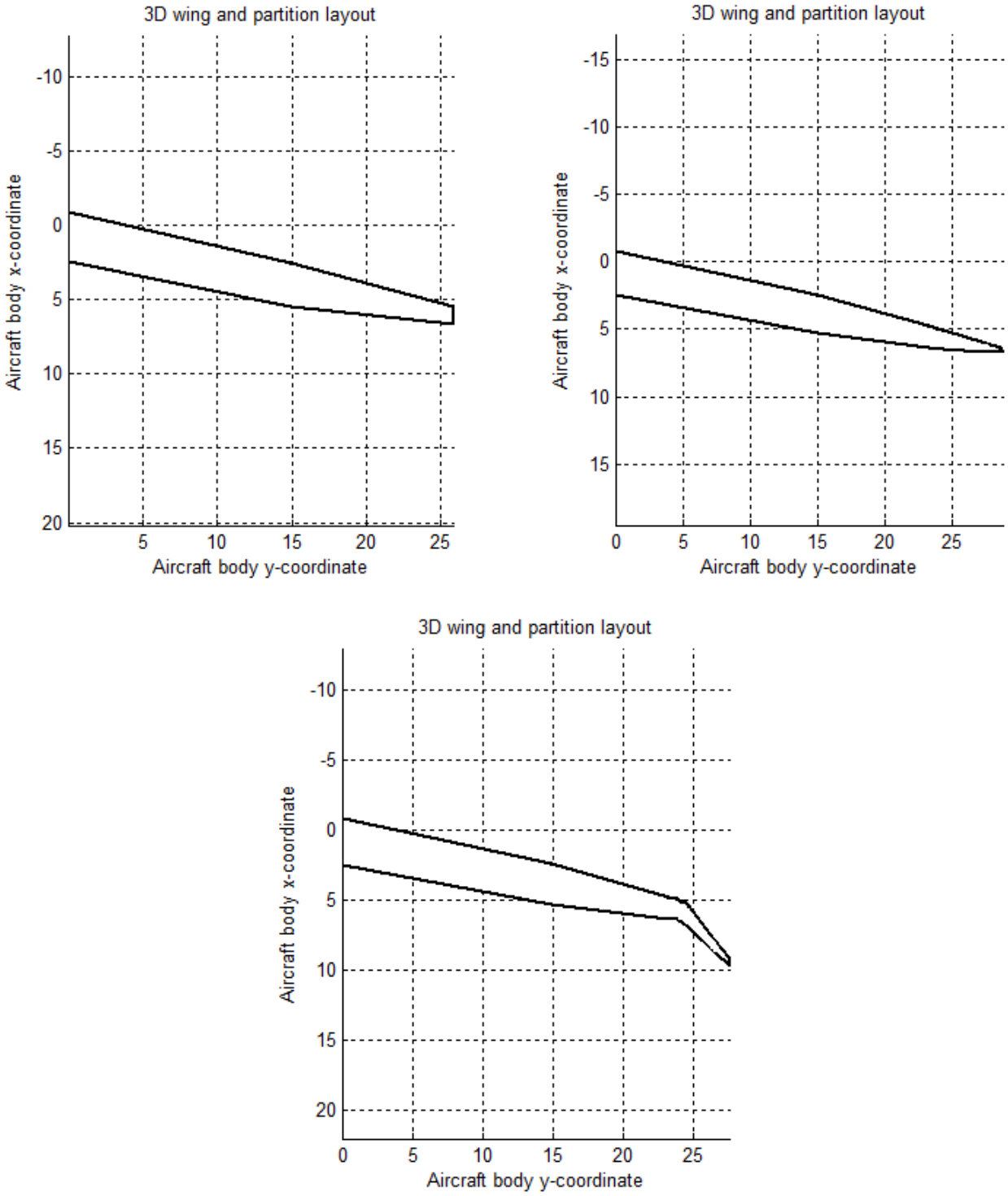

Figure 5 – *Tornado* Clean Wing Models (Half Span Only, dimensions in meters)

Top Left: Baseline SUGAR Wing
Top Right: SUGAR Main Wing with Unswept VGRWT/NCE Tip
Bottom: SUGAR Main Wing with Fully-Swept VGRWT/NCE Tip

2.4.2 Fluent Models

Similar to *Tornado*, wing models were constructed in DesignModeler to match the data provided by Boeing. Due to the time constraint imposed by CFD analysis, only one half of the wing planform was modeled. The mesh consists of tetrahedral elements, with a minimum size of 1 mm. Further, the curvature angle and proximity was set to the lowest possible setting to ensure a quality mesh. With these settings, all starting models contained approximately 6 million elements. After the completion of adaptive gridding, the models consisted of nearly 8 million elements. This process will be discussed further in Chapter 3. The wing models used are shown as Figure 6 with meshing overlaid before the adaptive gridding process commenced.

The fluid volume used to simulate the flow is a half circle, with one wall at the wing root and the other extending approximately 10 chord lengths past the wingtip. Similarly, the front and rear boundary also clear the leading and trailing edge by at least 10 chord lengths. The front face was set to be a pressure inlet, while the rear face is a pressure outlet. The left and right boundaries were set to be symmetry walls.

In order to obtain a fair comparison to the *Tornado* results, *Fluent* ran inviscid calculations with the energy equation enabled to simulate compressible flow. Using a six-core machine, each iteration took approximately 3 to 4 hours to complete. As with *Tornado*, the step between the main wing and the VGRWT/NCE tip was not modeled due to the complexity of the mechanism and the difficulty of obtaining a quality mesh over a very small step.

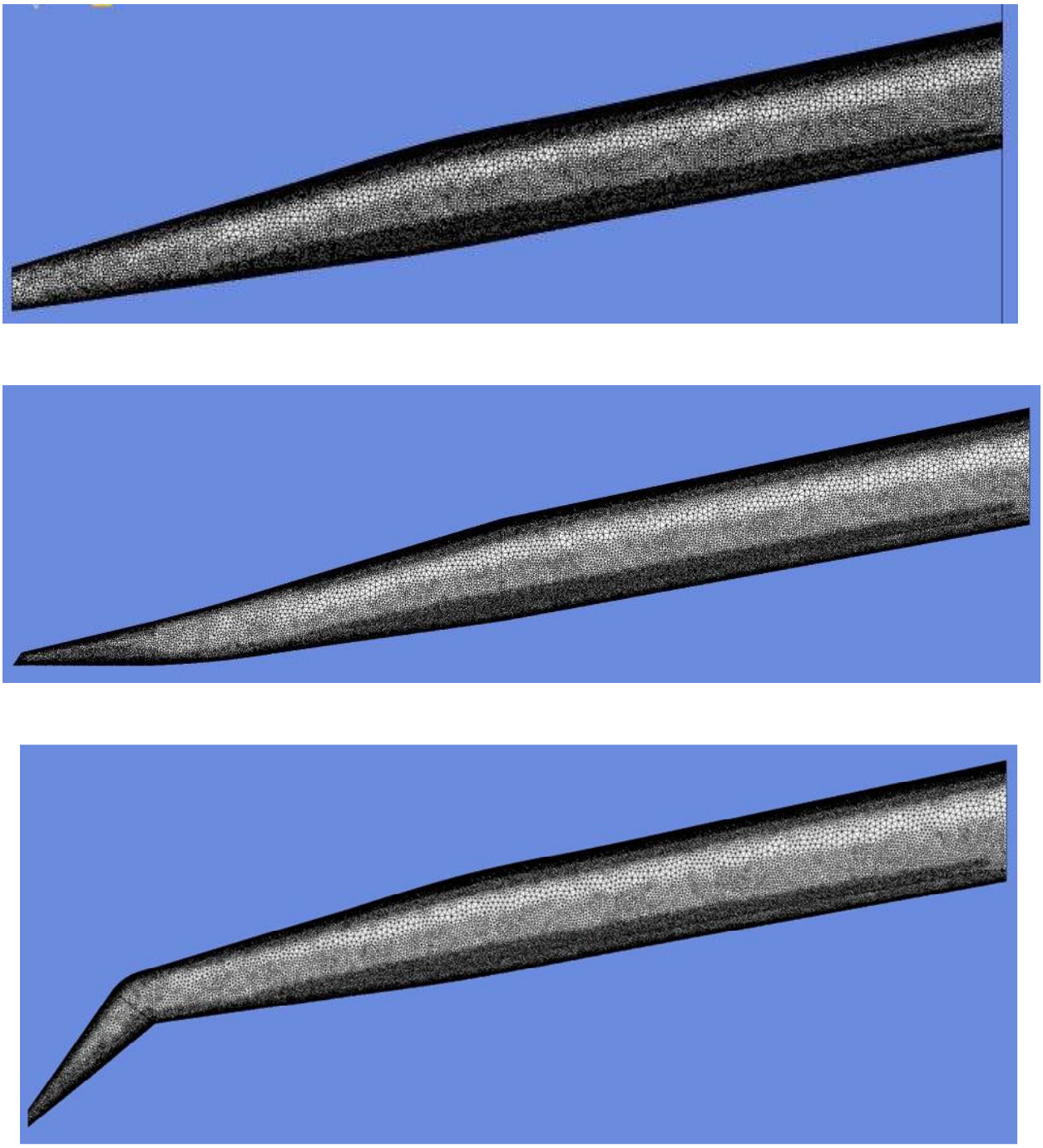

Figure 6 – *Fluent* Clean Wing Models Before Adaptation

Top: Baseline SUGAR Main Wing
Middle: SUGAR Wing with Unswept VGRWT/NCE Tip
Bottom: SUGAR Wing with Fully-Swept VGRWT/NCE Tip

2.5 Wing Models with Strut and Jury

The baseline SUGAR wing incorporates a truss-braced system in its design, therefore a complete wing system was modeled to gain a true understanding of performance. The strut and jury were constructed from data provided by Boeing from previously completed SUGAR MDO analysis. Boeing specified that the strut and jury be non-lifting, therefore the airfoil shape was assumed to be a symmetric NACA 4-digit airfoil of thickness specified by the MDO analysis. Figure 7 provides a view of the modeled full SUGAR TBW wing configuration, while Table 3 summarizes the geometry of the strut and jury. Figure 8 shows details of the strut and jury model. In order to evaluate the performance of the VGRWT/NCE tip against the baseline SUGAR tip, an aileron was added. Assumed to be 25% of chord, the aileron was allowed a typical maximum deflection of ±20°. The length of the aileron was determined from existing passenger aircraft and set to be approximately 10 ft. In addition to the unswept and fully-swept cases, models of intermediate sweep were constructed to give a full picture of the VGRWT/NCE tip performance throughout the sweep range. These additional models reflect quarter-sweep, half-sweep, and three-quarter sweep positions. The area of the wing planform across the models was consistent, with a maximum deviation of approximately 0.45 ft^2.

In order to truly isolate the performance of the tip, force data was extracted from *Tornado* for each VLM panel outboard of the 939 inch span station. Since the inboard profile did not change, Figure 9, 10, and 11 show the detail of the tip treatment for each sweep case and the baseline SUGAR case. The area considered in the tip calculations is shaded in each figure.

Table 3 – Geometry of Strut and Jury

	Strut	Jury
Span, ft	49.08	4.76
Root Chord, ft	3.44	1.06
Tip Chord, ft	4.00	1.06
Sweep, deg	8.85	-7.29
Dihedral, deg	15.3	88.77

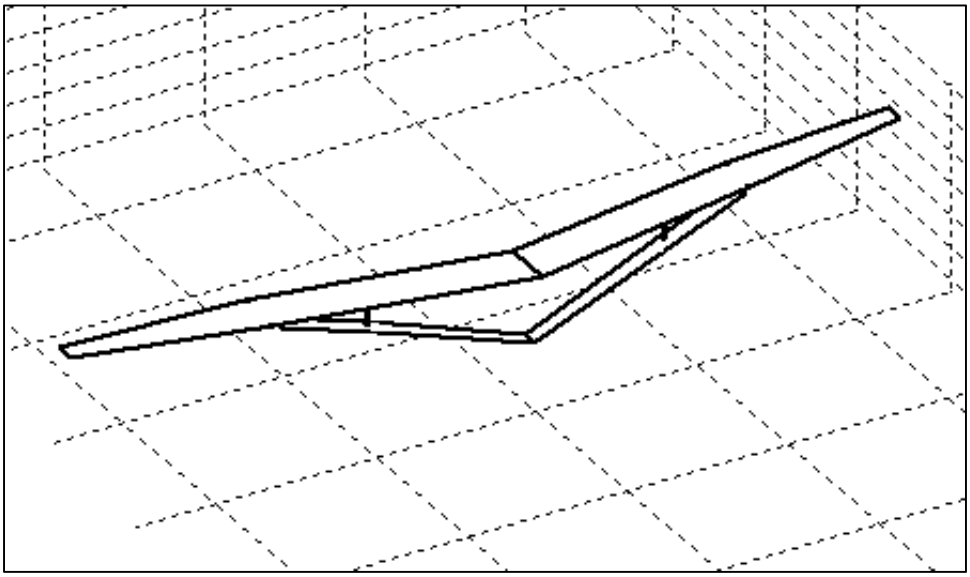

Figure 7 – Full Configuration with Strut and Jury

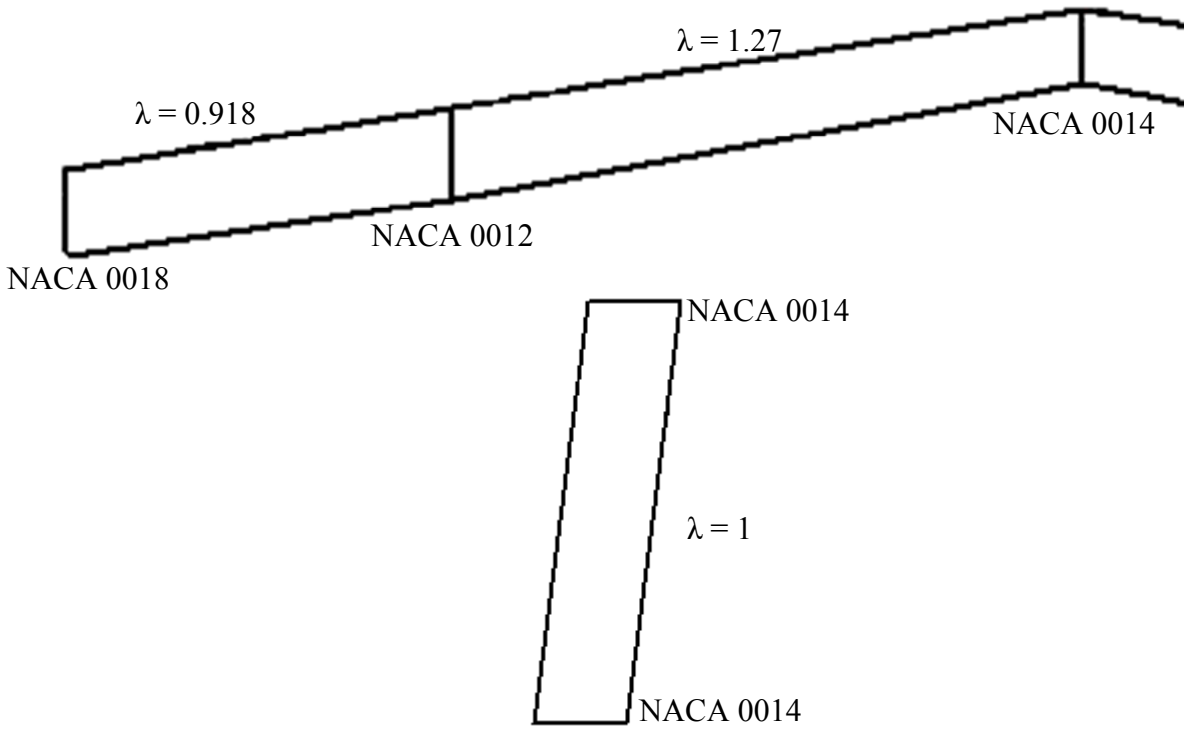

Figure 8 – Details of Strut (Top) and Jury (Bottom) *Tornado* Models (λ = taper ratio)

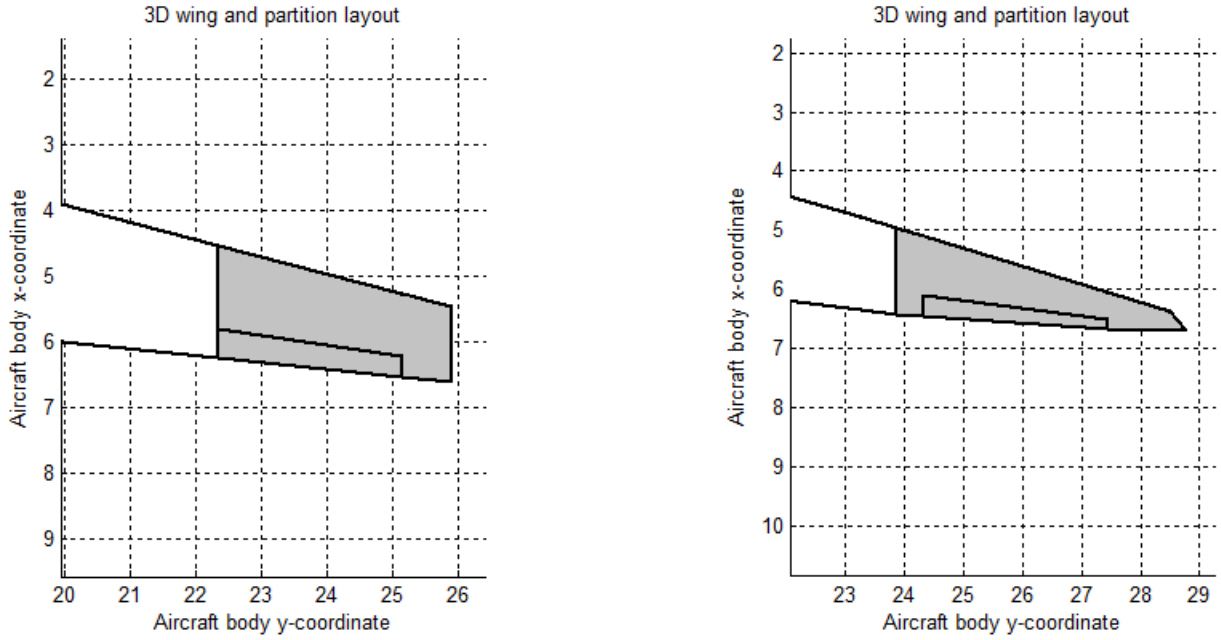

Figure 9 – Baseline SUGAR (Left) and Unswept (Right) VGRWT/NCE Tip Details Dimensions in meters, tip areas for comparison are shaded

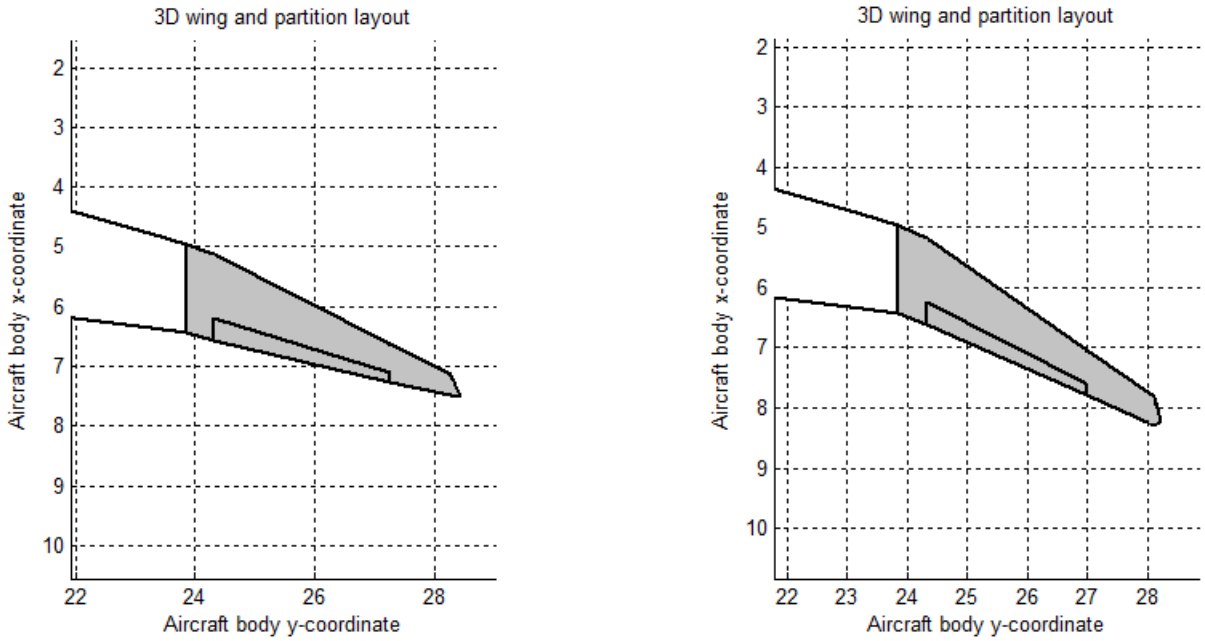

Figure 10 – Quarter-Sweep (Left) and Half-Sweep (Right) VGRWT/NCE Tip Details
Dimensions in meters, tip areas for comparison are shaded

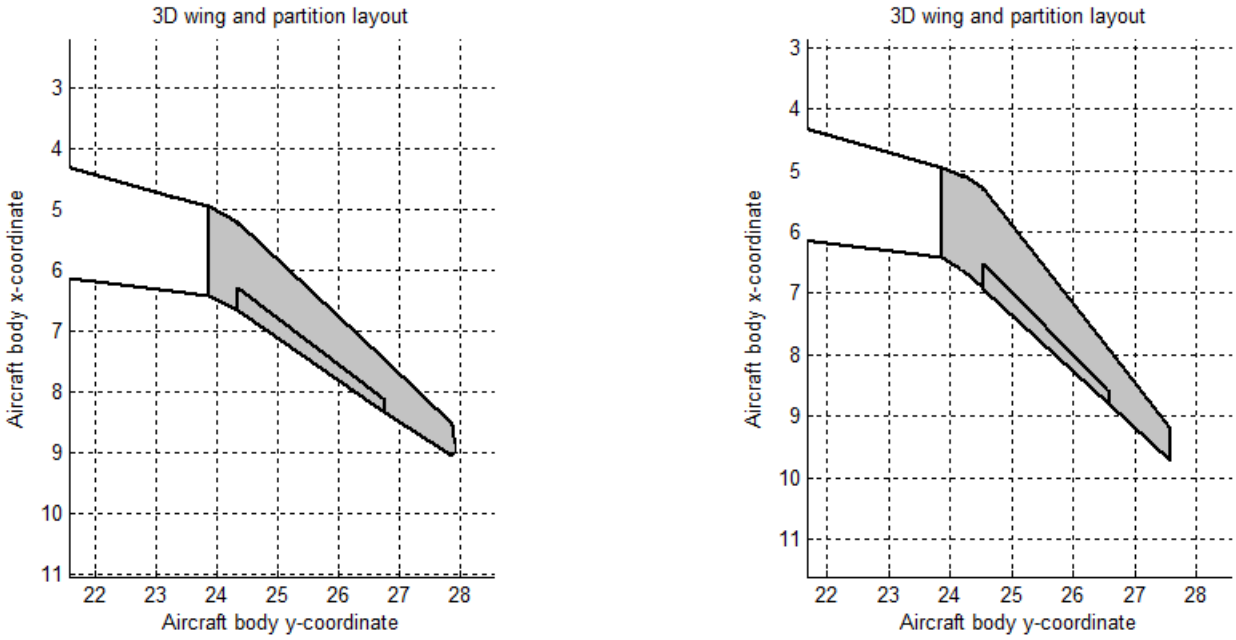

Figure 11 – Three-Quarter (Left) and Full-Sweep (Right) VGRWT/NCE Tip Details
Dimensions in meters, tip areas for comparison are shaded

Chapter 3: Results and Discussion

3.1 Clean Wing Results

The first stage of analysis centered on comparing the performance of the unmodified baseline SUGAR main wing with that of the SUGAR wing incorporating the VGRWT/NCE wingtip. The full wing models described in Section 2.4.1 were used for this examination. The simulations were run at cruise conditions, Mach 0.7 and 44,000 ft altitude. Also, the design cruise lift coefficient of the baseline SUGAR wing is 0.7. Therefore, the incidence angle of the wing was adjusted for each case in order to maintain this value within a reasonable tolerance.

3.1.1 Tornado Results

The *Tornado* results for the clean wing (no strut or jury) configurations are summarized as Table 4. In order to maintain nearly the same C_L for each configuration, the incidence angle only needed to decrease by approximately a quarter degree. For the same lift coefficient, the VGRWT/NCE configurations produce more total lift than the baseline SUGAR main wing. The difference for both the unswept and fully-swept case is approximately 2,800 lb. This is largely due to the increase in span and area that the wingtip provides. Furthermore, the unswept tip provides slightly more lift than the fully-swept configuration as intended, since the VGRWT/NCE will be unswept during take-off. The pitching moment coefficient also increases slightly after the VGRWT/NCE tip is added. This is expected as the increased area should increase the stability of the aircraft. No drag results were included in Table 4 due to the fact that *Tornado* is an inviscid code. A method for viscous drag estimation will be discussed in Section 3.1.4.

Table 4 – *Tornado* Results for Clean Wing Configurations

Configuration	Baseline SUGAR Main Wing	SUGAR Wing with Unswept VGRWT/NCE Tip	SUGAR Wing with Fully-Swept VGRWT/NCE Tip
Incidence Angle (deg)	2.95	2.7	2.75
Total Lift (lb)	114,950	117,800	117,775
$\mathbf{C_L}$	0.702	0.702	0.703
$\mathbf{C_{M_{c/4}}}$	-0.71	-0.75	-0.74

3.1.2 Fluent Results

In order to verify the results obtained by *Tornado*, CFD analysis was conducted using *ANSYS Fluent*. As described in Section 2.4.2, inviscid simulations were conducted and adaptive gridding was required to ensure converged results. After a run was completed and a lift coefficient had converged, the grid was adapted based on pressure gradients. Then, the simulation was run again, and the process was repeated until there was convergence between runs. Initial runs consisted of 1000 iterations, with subsequent runs consisting of 500 iterations. Figure 12 shows a plot of this process for the unswept VGRWT/NCE tip case. Plots were created for the baseline SUGAR and fully-swept cases but are not included due to redundancy. Figure 13 shows details of the grid at the wing root before and after the adaption occurred. Similar to Figure 12, this is also for the unswept case. Again, figures for the baseline SUGAR and fully-swept tip cases are not included due to the similarity between all configurations.

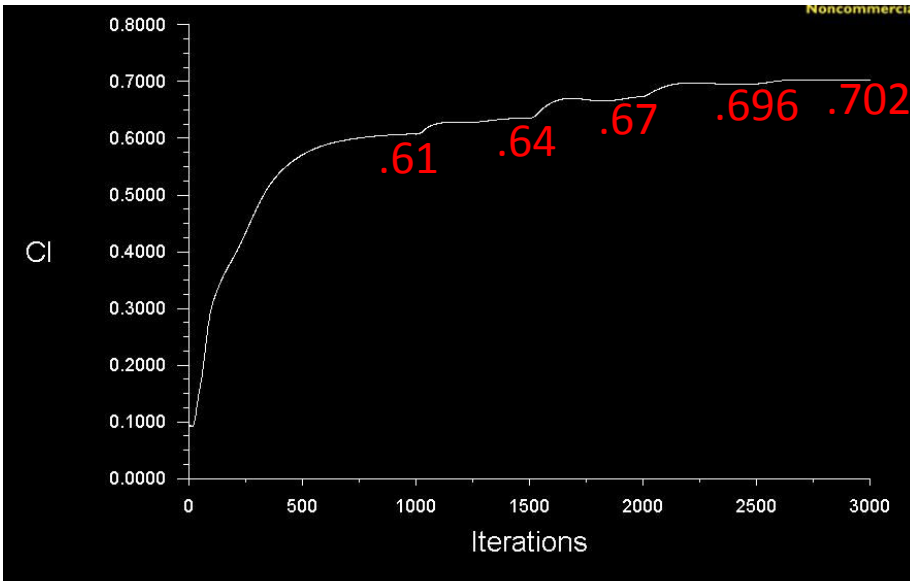

Figure 12 – Adaptive Gridding Convergence for Unswept VGRWT/NCE Tip Case (C_L in red)

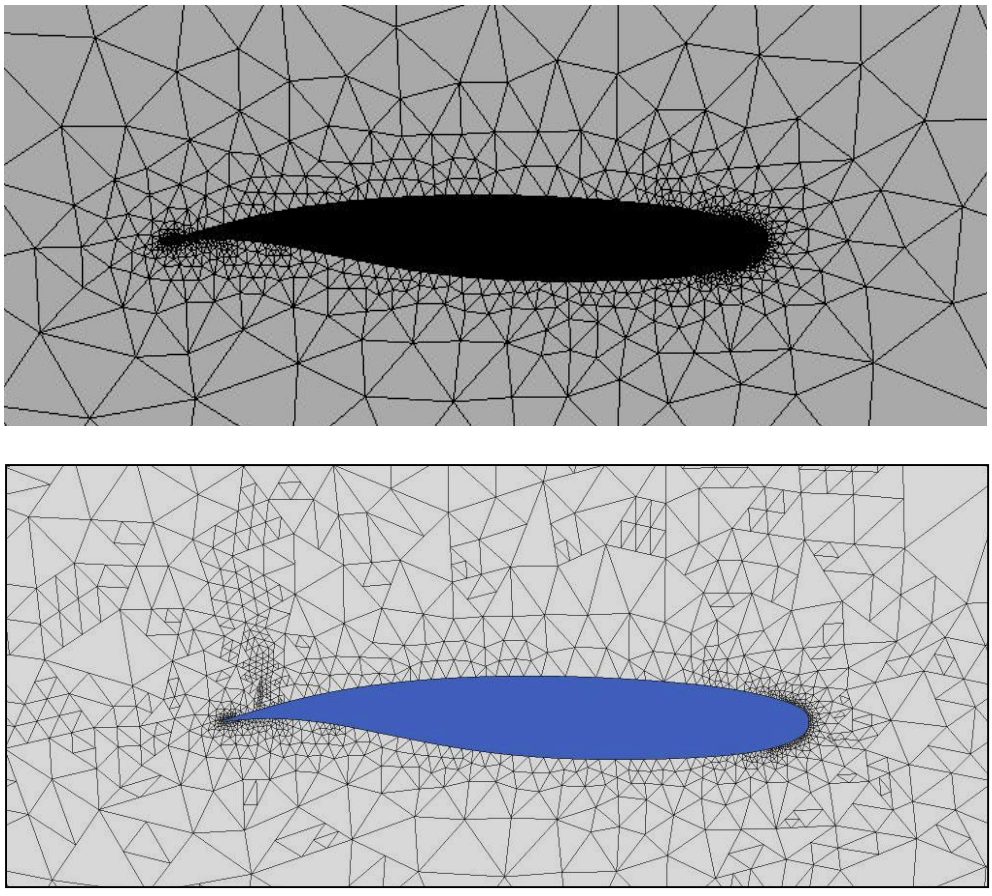

Figure 13 – Grids at the Wing Root for Unswept VGRWT/NCE Tip Case (Top – Original Grid; Bottom – Final Adapted Grid)

Once the adaptive gridding was completed, suitable simulations were run, and final results are presented as Table 5. The VGRWT/NCE configurations again produce more lift than the unmodified SUGAR wing and also produce an increased moment coefficient. Figures 14 to 16 show pressure contour plots of the various configurations. A large region of low pressure is evident near the trailing edge, which suggests a region of supersonic flow over approximately 75% of the span. This is confirmed by velocity contours shown as Figure 17. The left picture shows a cut at the wing root, where a large supersonic region is evident, however at the 939 inch span station which corresponds to the main wing/VGRWT/NCE tip junction, there is no supersonic flow. This is consistent for all configurations and further facilitates the incorporation of the VGRWT/NCE tip, since locally supersonic flow will not be a concern. Finally, the streamlines over the wing are shown as Figure 18. The streamlines remain relatively straight over the entire span and suggest that the sweeping tip will not contribute large amounts of turbulent flow over the airfoil.

Table 5 – *Fluent* Results for Clean Wing Configurations

Configuration	**Baseline SUGAR Main Wing**	**SUGAR Wing with Unswept VGRWT/NCE Tip**	**SUGAR Wing with Fully-Swept VGRWT/NCE Tip**
Incidence Angle (deg)	2.8	2.8	2.8
Total Lift (lb)	115,500	118,190	118,500
$\mathbf{C_L}$	0.700	0.702	0.704
$\mathbf{C_{M_{c/4}}}$	-0.78	-0.795	-0.81

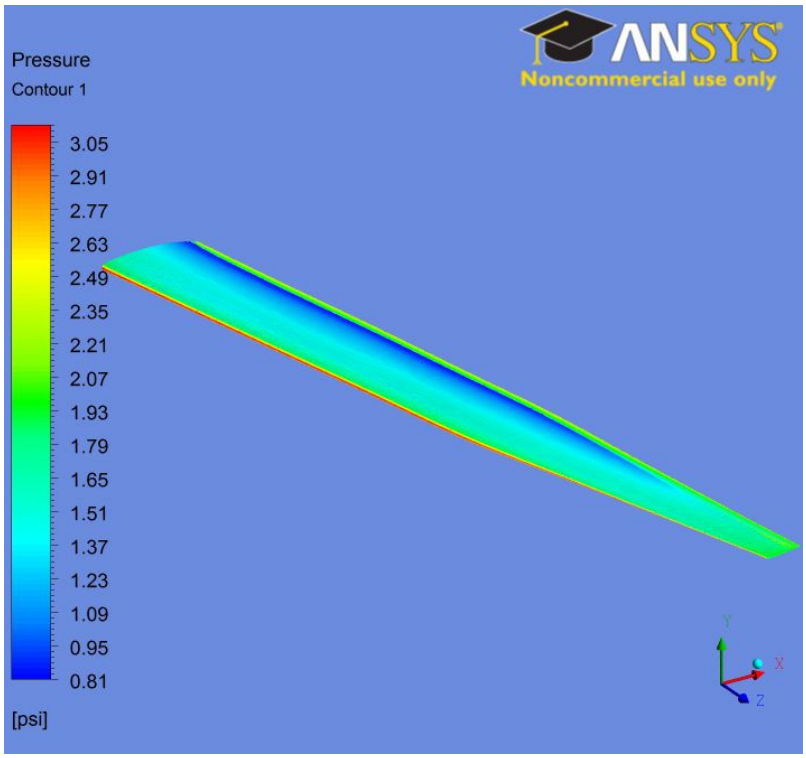

Figure 14 – Fluent Prediction of Top Surface Pressure Contours of Baseline SUGAR Main Wing

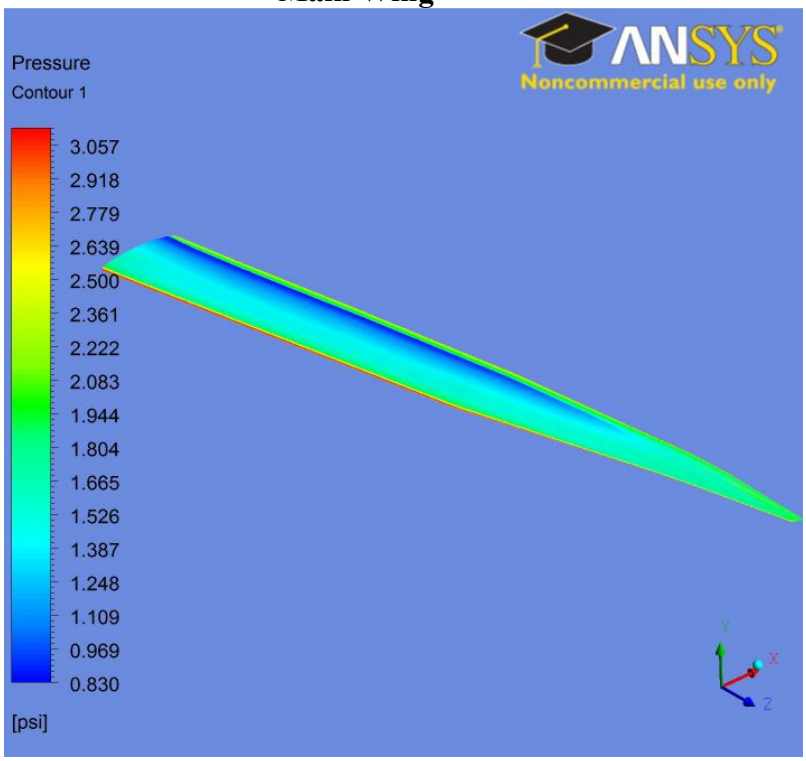

Figure 15 – Fluent Prediction of Top Surface Pressure Contours of SUGAR Wing with Unswept VGRWT/NCE Tip

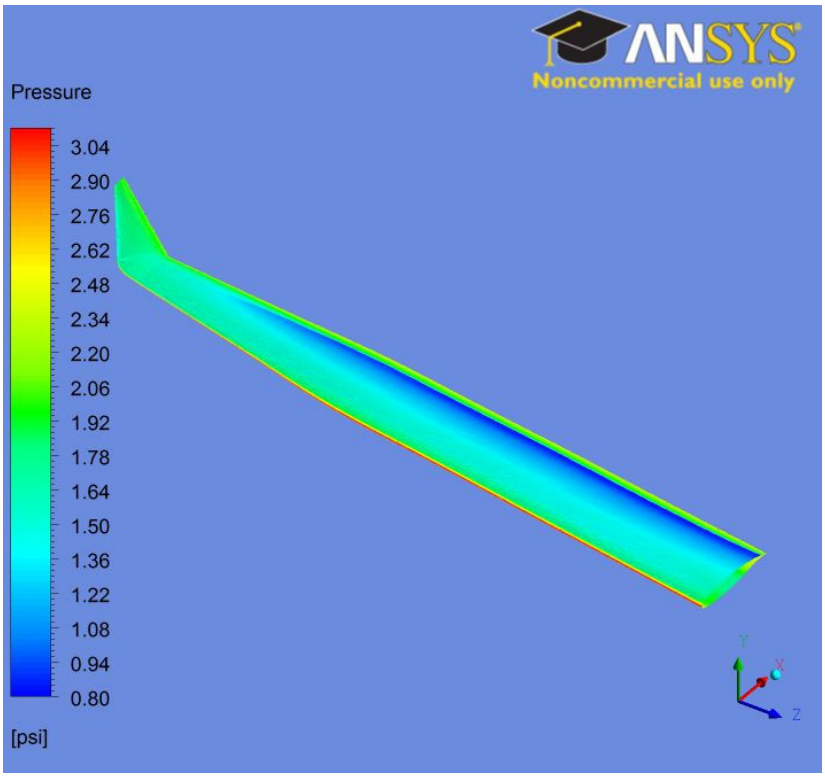

Figure 16 – Fluent Prediction of Top Surface Pressure Contours of SUGAR Wing with Fully-Swept VGRWT/NCE Tip

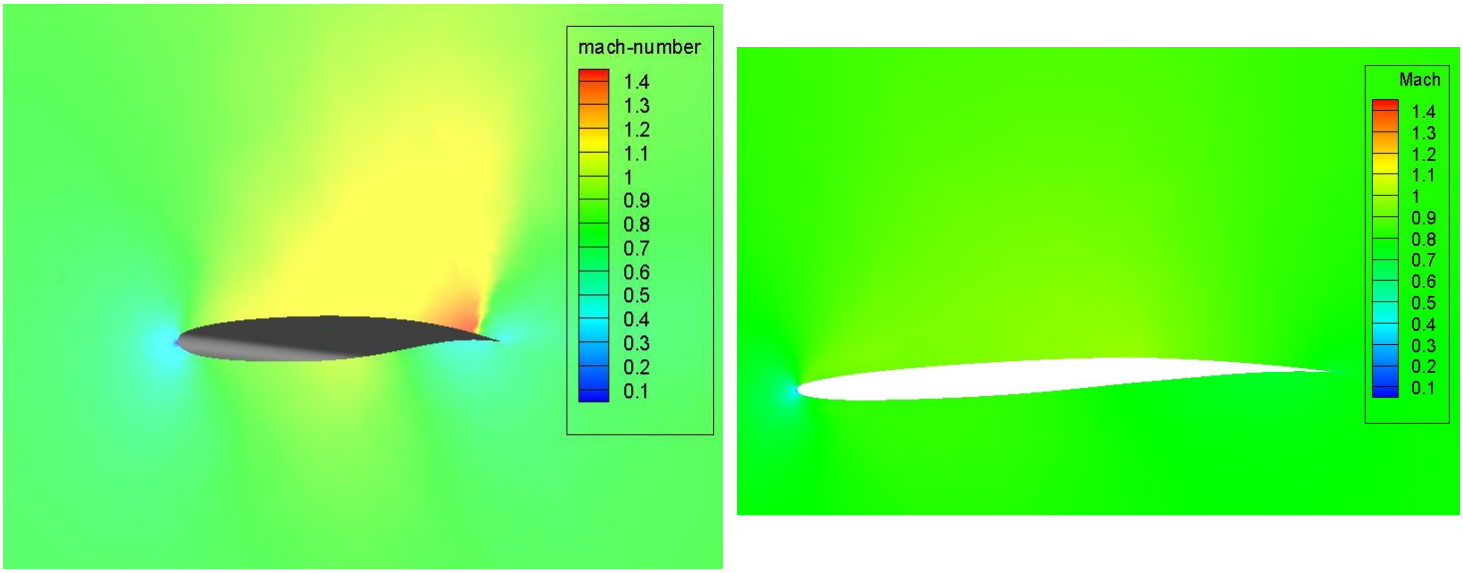

Figure 17 – Fluent Prediction of Velocity Profile at Wing Root (Left) and Main Wing/VGRWT Junction (Right)

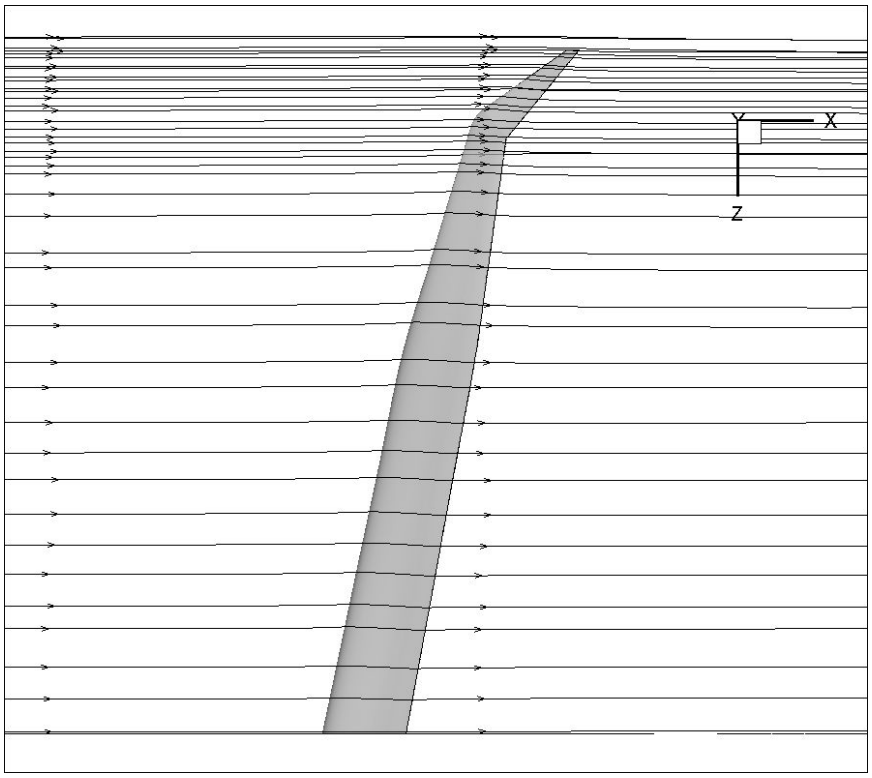

Figure 18 – Fluent Prediction of Streamlines Over SUGAR Wing with Fully-Swept VGRWT/NCE Tip

3.1.3 Comparison of Results

Table 6 summarizes the data obtained by both the VLM (*Tornado*) and CFD (*Fluent*) methods of analysis. The results generally agree across all areas of comparison. Since the lift coefficient was forced to be close to 0.7, the lift forces generated by each method should be comparable. Indeed, both *Fluent* and *Tornado* show that the VGRWT/NCE configurations produce approximately 2,800 lb of additional lift compared to the unmodified configuration. Also, the *Fluent* results show approximately 500 lb of additional lift over the *Tornado* results for all cases. *Fluent* shows a more consistent incidence angle across configurations, but the difference between methods is approximately one-tenth of a degree, which again shows excellent agreement. Finally, the *Fluent* results give an approximate 9% higher pitching moment coefficient for each configuration. Since CFD calculations of moment coefficients are generally

regarded as more accurate than those of VLM methods, this small difference is seen as a positive result and gives confidence in *Tornado*'s moment predictions moving forward. With corroborating CFD results, it has been shown that VLM predictions are very useful in early design analysis and are capable of giving acceptably accurate results. One could use CFD results like these obtained here to develop a correction to the VLM results, but that was not deemed worthwhile. With this in mind, the analysis of the forces and moments produced solely by the wingtips was conducted with *Tornado* alone.

Table 6 – Comparison of *Tornado* and *Fluent* Results for Clean Wing Cases

	Fluent	***Tornado***	***Fluent***	***Tornado***	***Fluent***	***Tornado***
Configuration	Baseline SUGAR Wing	Baseline SUGAR Wing	SUGAR Wing with Unswept VGRWT/ NCE Tip	SUGAR Wing with Unswept VGRWT/ NCE Tip	SUGAR Wing with Fully-Swept VGRWT/ NCE Tip	SUGAR Wing with Fully-Swept VGRWT/ NCE Tip
Incidence Angle (deg)	2.8	2.95	2.8	2.7	2.8	2.75
Total Lift (lb)	115,500	114,950	118,190	117,800	118,500	117,775
$\mathbf{C_L}$	0.700	0.702	0.702	0.702	0.704	0.703
$\mathbf{C_{M_{c/4}}}$	-0.78	-0.71	-.795	-0.75	-0.81	-0.74

3.1.4 Viscous Drag Estimation

In order to determine the effect that the VGRWT/NCE has on the baseline SUGAR planform, a viscous drag estimation was conducted. Equation 1 shows the drag coefficient in the usual way:

$$C_D = C_{D0} + \frac{C_L^2}{\pi ARe} \tag{1}$$

The Oswald efficiency factor, *e*, is given by Equation 2, and incorporates a high aspect ratio correction.

$$e = \frac{1}{\pi ARk + \frac{1}{us}} \tag{2}$$

The viscous drag due to lift factor, *k*, is a function of wing sweep and C_{D0}, and the induced drag due to the fuselage, *s*, is a function of span and fuselage diameter. Finally, the planform efficiency factor, *u*, is assumed to be 0.99 [13]. The zero-lift drag, C_{D0}, was computed by *Tornado* which employs conventional low-order methods. Using this method, the total drag coefficient was determined for each configuration and is shown as Table 7. The VGRWT/NCE configurations show a reduced drag compared to the baseline SUGAR planform. This is largely due to the increased aspect ratio brought on by the addition of the VGRWT/NCE tip. Also, the highest lift to drag ratio is achieved by the unswept tip configuration, a feature which will be beneficial during take-off and landing. Finally, the zero lift-drag computed by *Tornado* is nearly identical across models due to the fact that approximately 90% of the planform is shared between configurations.

Table 7 – Viscous Drag Estimation for Each Configuration

Configuration	Baseline SUGAR Wing	SUGAR Wing with Unswept VGRWT/NCE Tip	SUGAR Wing with Fully- Swept VGRWT/NCE Tip
C_{D0}	0.00889	0.00889	0.00882
Oswald Efficiency Factor	0.81	0.79	0.80
C_D	0.0187	0.0173	0.0178
L/D	37.4	40.4	39.2

3.2 Force and Moment Results on the Various Wingtips

The second stage of analysis focused on calculating the forces and moments generated by the respective wingtips themselves. In order to obtain a full understanding of the influence of the tips on the wing system, the strut and jury was added as described in Section 2.5. All tests were run at Mach 0.7, 44,000 ft altitude, and the incidence angle was varied in order to maintain a lift coefficient of 0.7 within reasonable tolerances.

3.2.1 Wingtip Results for All Configurations

Tornado calculates force data on each panel during every simulation. This data was extracted for panels existing on the wingtip and reduced to an equivalent point force on the wingtip. The force data presented is a resultant force of the lift, drag and side force. However, the drag and side force are consistently an order of magnitude less than the lift force. Therefore, the resultant force is overwhelming comprised of lift. The moment generated by each tip was calculated by multiplying this resultant force with its distance to the elastic axis of the main

wing. The elastic axis was taken to be constant at 40% chord of the main wing, and it was assumed to be unaffected by the orientation of the VGRWT/NCE tip. Finally, the aileron was rotated through ±20° to determine its effect on the moment. Figures 19, 20 and 21 show the location of the resultant force for each tip, along with the elastic axis. The location of the resultant point force did not vary appreciably with aileron deflection, therefore the locations, indicated as a red dot, are presented for the undeflected case. As in Section 2.5, the shaded grey area is the area considered for tip calculations. Figure 22 shows the force generated by each tip as a function of aileron deflection. Similarly, Figure 23 shows the moment generated as a function of aileron deflection.

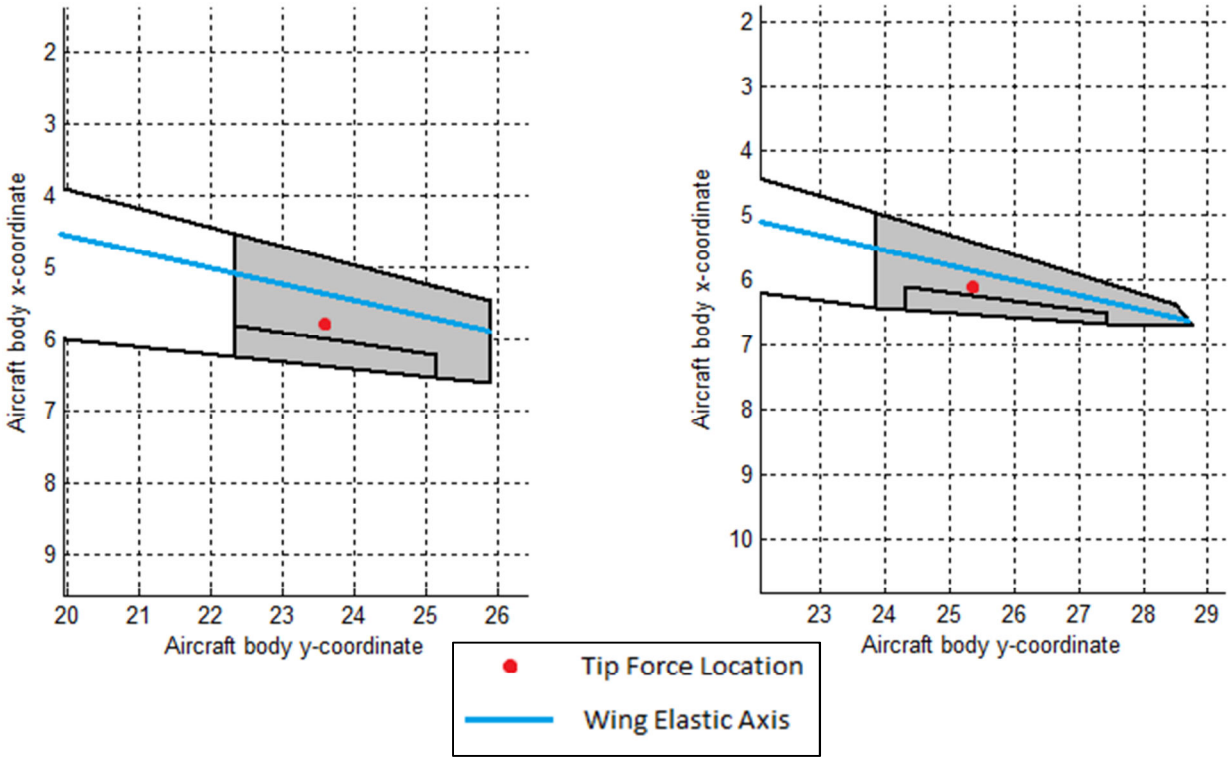

Figure 19 – Baseline SUGAR Tip (Left) and Unswept VGRWT/NCE Tip (Right) Force Location (Dimensions in meters)

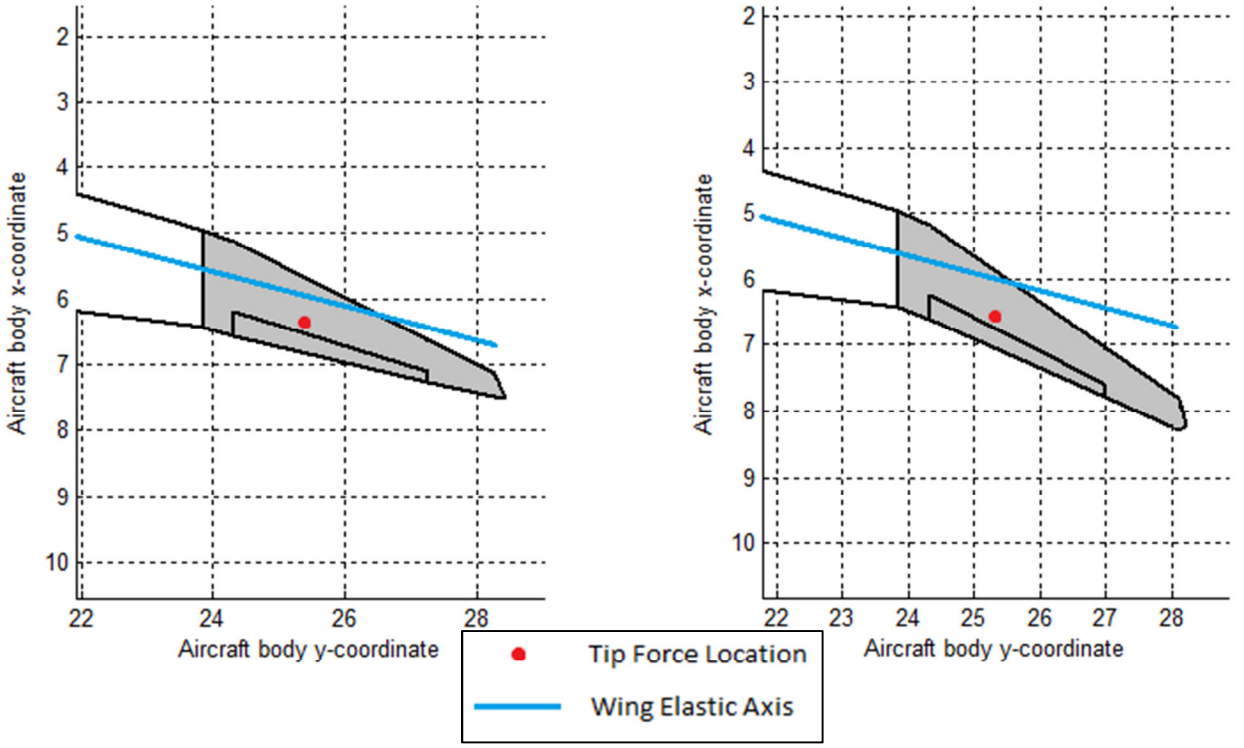

Figure 20 – Quarter-Sweep VGRWT/NCE Tip (Left) and Half-Sweep VGRWT/NCE Tip (Right) Force Location (Dimensions in meters)

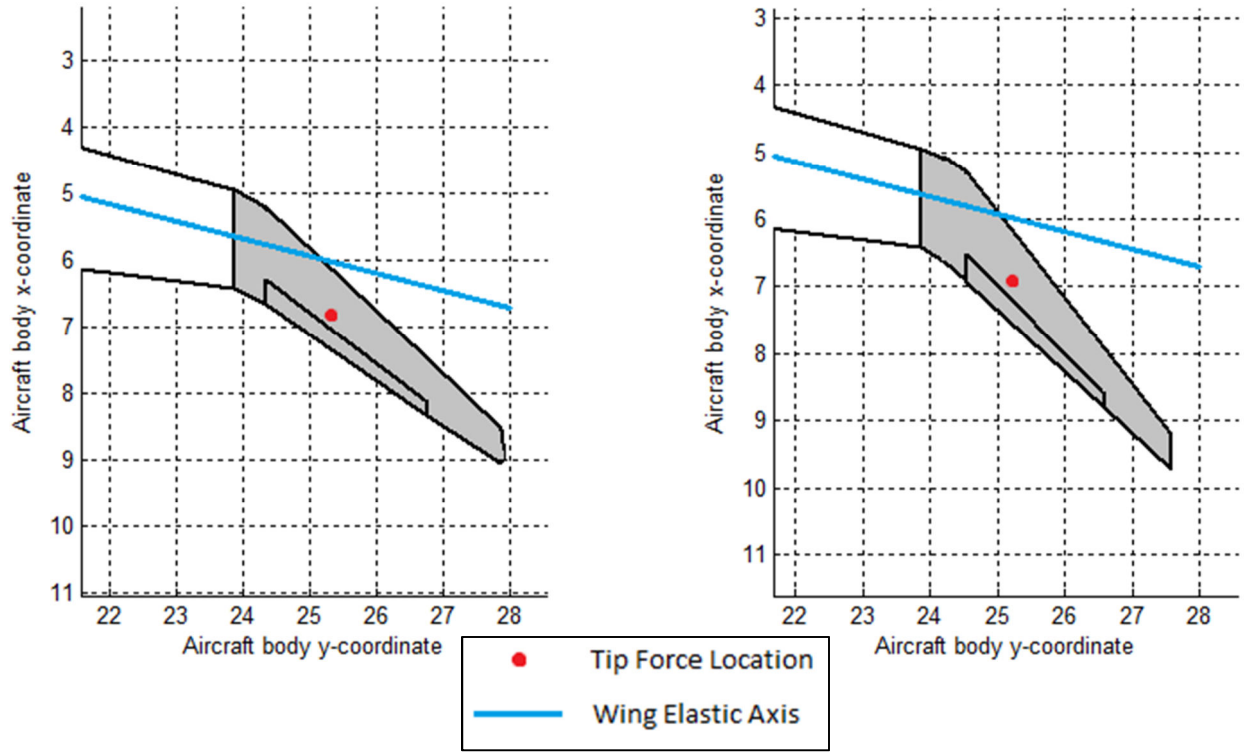

Figure 21 – Three-Quarter Sweep VGRWT/NCE Tip (Left) and Full-Sweep VGRWT/NCE Tip (Right) Force Location (Dimensions in meters)

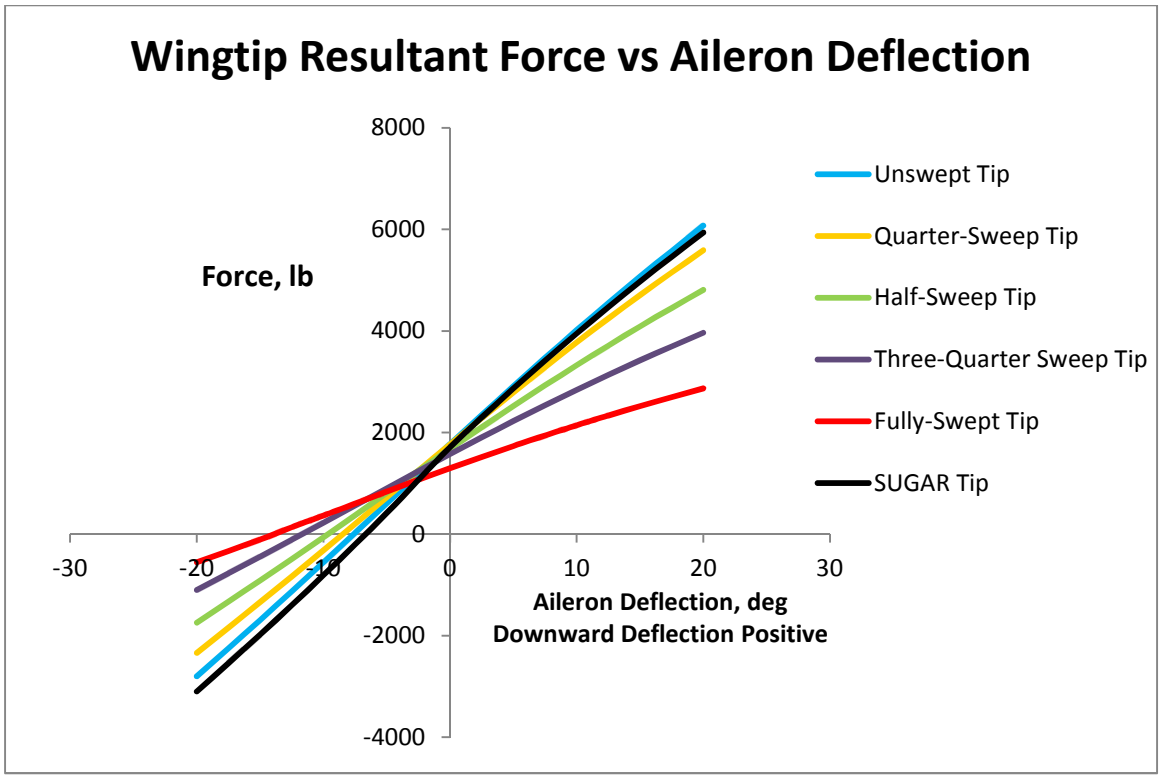

Figure 22 – Wingtip Resultant Force as a Function of Sweep and Aileron Deflection

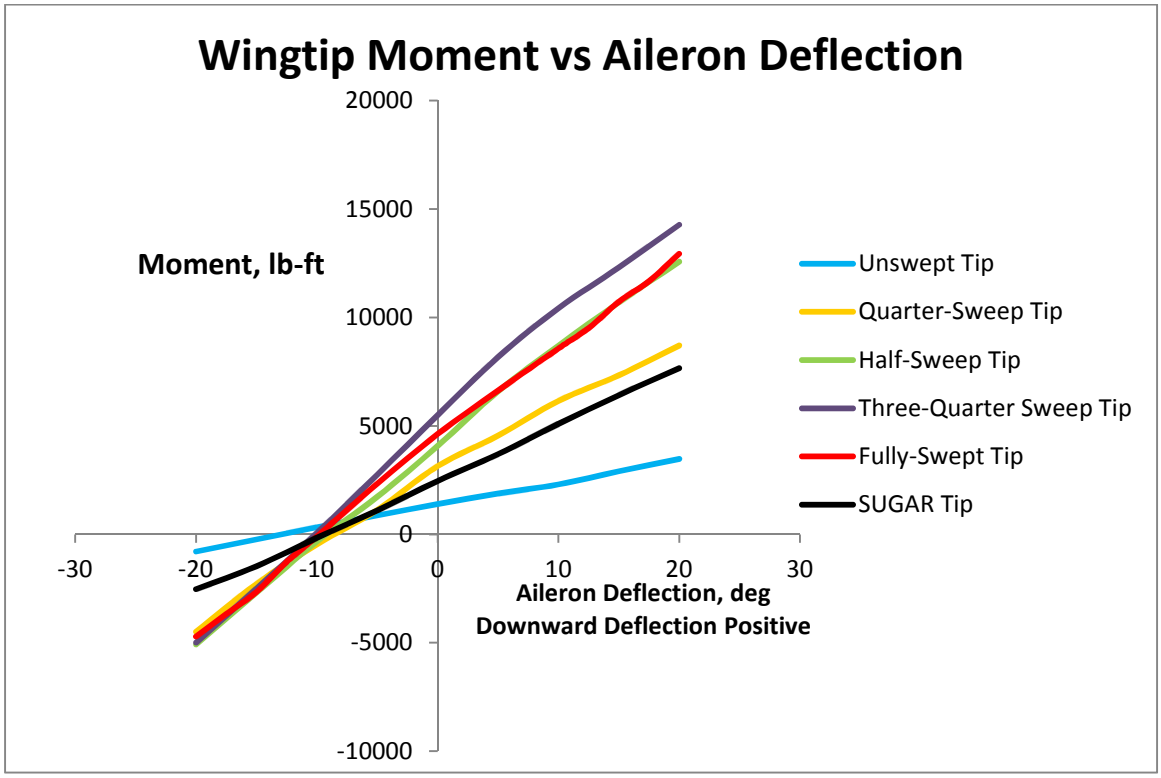

Figure 23 – Wingtip Moment as a Function of Sweep and Aileron Deflection

From Figure 22, it can be seen that the performance of the unswept tip closely mirrors that of the SUGAR tip. This was the intention of the unswept tip design and successfully validates the modeling procedure outlined in Section 2.3. Also, the force generated by each wingtip decreases as the sweep angle increases. This was expected since highly-swept wings generate less lift than slightly-swept wings. While the difference in force produced between the unswept and swept tip cases is quite large at the extremes of aileron deflection, they are quite small at the neutral aileron position. The difference in the force generated for an undeflected aileron is approximately 450 lb per tip, which is a small variation considering each half of the wing produces nearly 60,000 lb of lift. Finally, the resultant forces generated for each VGRWT/NCE tip behave in a linear manner with respect to aileron deflection. This is to be expected, since the absolute value of the force produced by the aileron will be approximately equal for both positive and negative deflections.

The behavior of the moments with respect to aileron deflection, given as Figure 23, shows that the swept tip cases produce larger moments than the unswept tip case. The quarter-sweep configuration produces moments that are most comparable to the baseline SUGAR tip, with the unswept tip case producing substantially less moment. This is due to the close proximity of the force location to the elastic axis for the unswept tip case, as shown by Figure 19. An interesting result is that the three-quarter sweep tip case produces the largest moment. While the moment arm is indeed less than the fully-swept tip case, as shown in Figure 21, the force produced by the three-quarter sweep tip configuration is much larger than that of the fully-swept tip case, as evidenced by Figure 22. Therefore, this larger force overwhelms the small difference in moment arm and produces a larger tip moment overall. We also see that the half-sweep and fully-swept tip cases produce nearly identical moment trends. As with the three-quarter sweep

case, this is due to the balance achieved by having a larger moment arm for the fully-swept tip case, but with a smaller force, compared to that of the half-swept tip case, which has a larger force, but a smaller moment arm. Finally, all of the moments produced by the neutral aileron position are positive. With the convention that positive moments are clockwise, this means that the tip will be attempting to pitch down, which is the desired result to resist divergence as well as having the entire aircraft return to a neutral position should it suddenly pitch up as a result of wind turbulence, for example.

3.2.2 Wingtip Performance Deltas

To measure the performance of each sweep configuration with respect to the baseline SUGAR tip, a simple "delta" analysis was conducted. The deltas for each configuration are found according to the following equations, where q is the dynamic pressure and A is the planform area of the respective wingtip sections:

$$\Delta C_{Force} = \frac{F_{Sweep} - F_{SUGAR}}{qA} \tag{3}$$

$$\Delta C_{Moment} = \frac{M_{Sweep} - M_{SUGAR}}{qA} \tag{4}$$

The graphical results of this analysis are presented as Figure 24 and Figure 25, respectively. The trends of these plots are broadly similar to Figure 22 and Figure 23 presented above.

Regarding the force delta plot, Figure 24, we can clearly see that the unswept tip provides very comparable performance to the baseline SUGAR tip, with a maximum delta coefficient of 0.048. The deltas for each configuration increase as the sweep angle increases, with the fully-swept tip providing the largest difference in force. For this configuration, the maximum delta coefficient occurs with the maximum aileron deflection angle and is approximately -0.49.

The moment delta plot, Figure 25, also shows similar behavior to Figure 22. We again see that the most comparable configuration to the baseline SUGAR tip is the quarter-sweep VGRWT/NCE tip case, for reasons outlined above. We also see that the maximum moment delta coefficient, approximately 1.05, is given by the three-quarter sweep VGRWT/NCE tip configuration, occurring again at maximum aileron deflection.

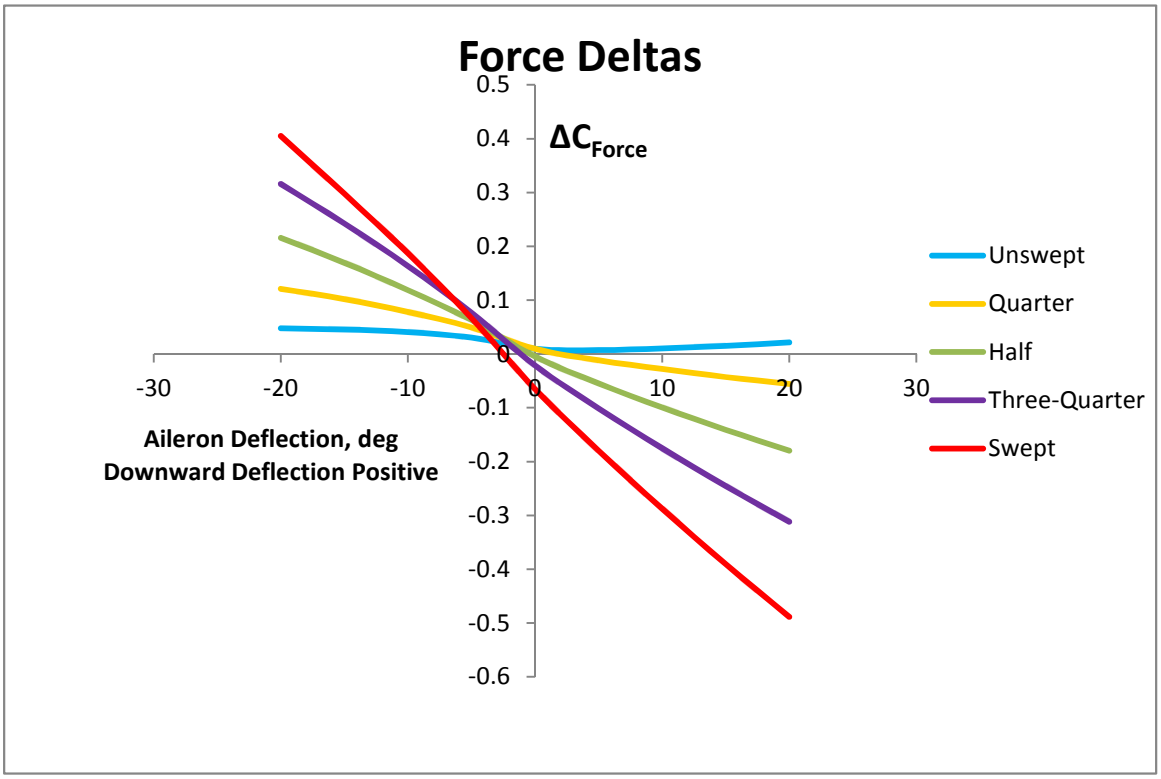

Figure 24 – Wingtip Force Coefficient Deltas for VGRWT/NCE Tip as a Function of Sweep and Aileron Deflection

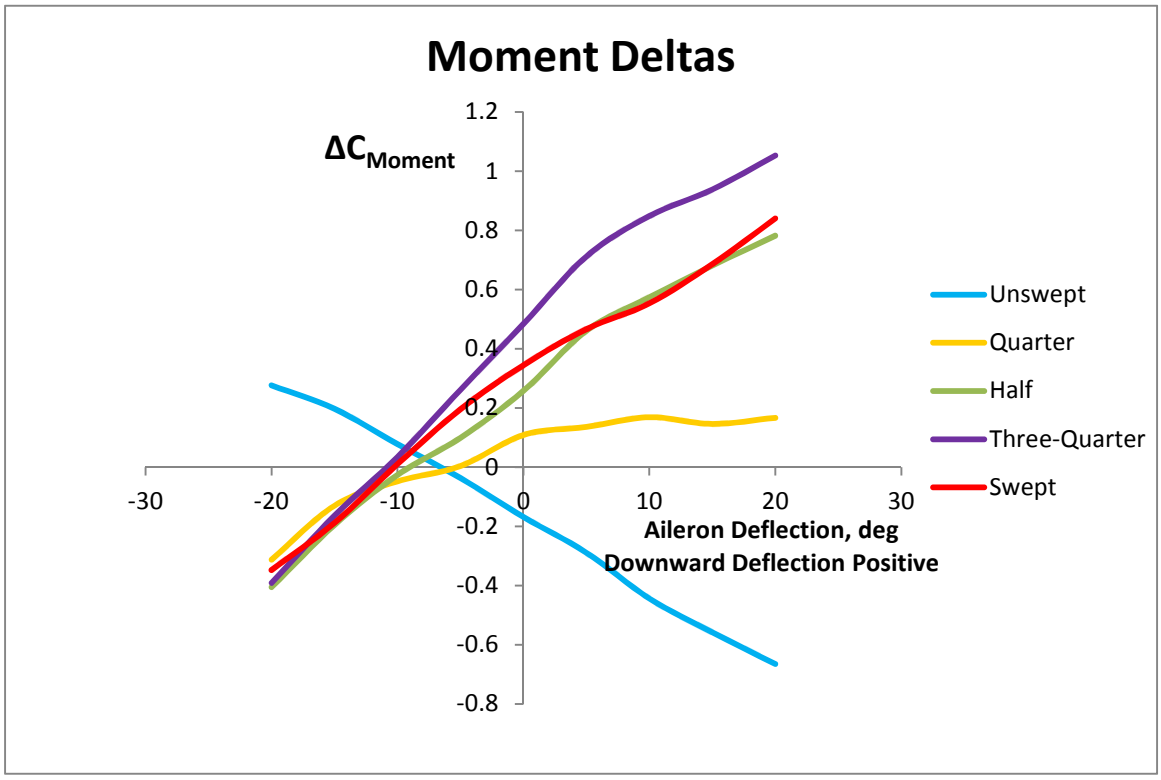

Figure 25 – Wingtip Moment Coefficient Deltas For VGRWT/NCE Tip as a Function of Sweep and Aileron Deflection

3.2.3 Wingtip Viscous Drag Estimation

A viscous drag estimation study was conducted on the wingtips alone similar to the procedure described in Section 3.1.4. Equation 1 was again used to find the viscous drag coefficient, and the zero-lift drag was calculated by *Tornado*. However, since the aspect ratio of the wingtips is low compared to the total wing, the Oswald efficiency factor was calculated according to the methods outlined in Raymer [14]. For wing sweep below 30°, e is given by:

$$e = 1.78(1 - 0.045 * AR^{0.68}) - 0.64 \quad (5)$$

For wing sweeps larger than 30°, it is given as:

$$e = 4.61(1 - 0.045 * AR^{0.68})(\cos \Lambda_{LE})^{0.15} - 3.1 \quad (6)$$

Using these methods, the viscous drag was calculated for the SUGAR, unswept and fully-swept VGRWT/NCE tip configurations. The intermediate sweeps were not analyzed due to the small

amount of time that will be spent in those transitional positions in flight. The results are presented in Table 8, and they show that the unswept VGRWT/NCE tip produces the lowest drag. Even though the tip area is the same, the unswept VGRWT/NCE tip has a larger span, which leads to a higher aspect ratio. This higher aspect ratio is largely the reason that the unswept tip produces the lowest drag, and consequently the highest L/D. As before, this would be helpful during take-off and landing, since lift is at a premium in those situations. The swept VGRWT/NCE tip also has a lower drag coefficient than the baseline SUGAR tip, suggesting it will be more efficient at cruise conditions than the baseline SUGAR tip. Finally, the viscous drag force calculated from these results was of the same order of magnitude as predicted by the *Tornado* inviscid drag calculations. Therefore, the resultant forces presented in Section 3.2.1 were not amended to reflect the viscous correction, since the effect on the resultant force would be small.

Table 8 – Viscous Drag Estimation on Various Wingtip Configurations

Configuration	**Baseline SUGAR Tip**	**Unswept VGRWT/NCE Tip**	**Fully-Swept VGRWT/NCE Tip**
C_{D0}	0.000549	0.000493	0.000426
Oswald Efficiency	0.99	0.86	0.74
C_D	0.0086	0.0063	0.0082
L/D	29.0	47.2	31.8

3.3 Drag Estimation of Flow Over Wing/VGRWT/NCE Tip Joint

As briefly mentioned in Chapter 2, the practical design of the VGRWT/NCE tip necessarily incorporates a small step between the main wing and the tip. As discussed in Section 2.3, portions of the tip must tuck into the main wing depending on the current orientation of the VGRWT/NCE tip. Therefore, the VGRWT/NCE tip is slightly thinner than the main wing, and drag issues due to the step must be addressed.

Figure 26 shows streamlines over the fully-swept VGRWT/NCE, with the approximate location of the step drawn in red. This shows that the streamlines over the step are generally straight. Considering the idealized case of an infinite swept wing, the components of the freestream can be decoupled according to Prandtl's independence principle. From this analysis, the normal component of flow is most important with regards to flow separation [15]. With the joint between the wing and VGRWT/NCE tip being nearly normal to the leading edge, taken to be 16° for this analysis, the normal component of the freestream flow over the step is M = 0.18. This is a low-speed flow, and compressibility effects would be negligible. Therefore, the results presented in Hoerner's classic drag reference, *Fluid Dynamic Drag* [16], are applicable to this case.

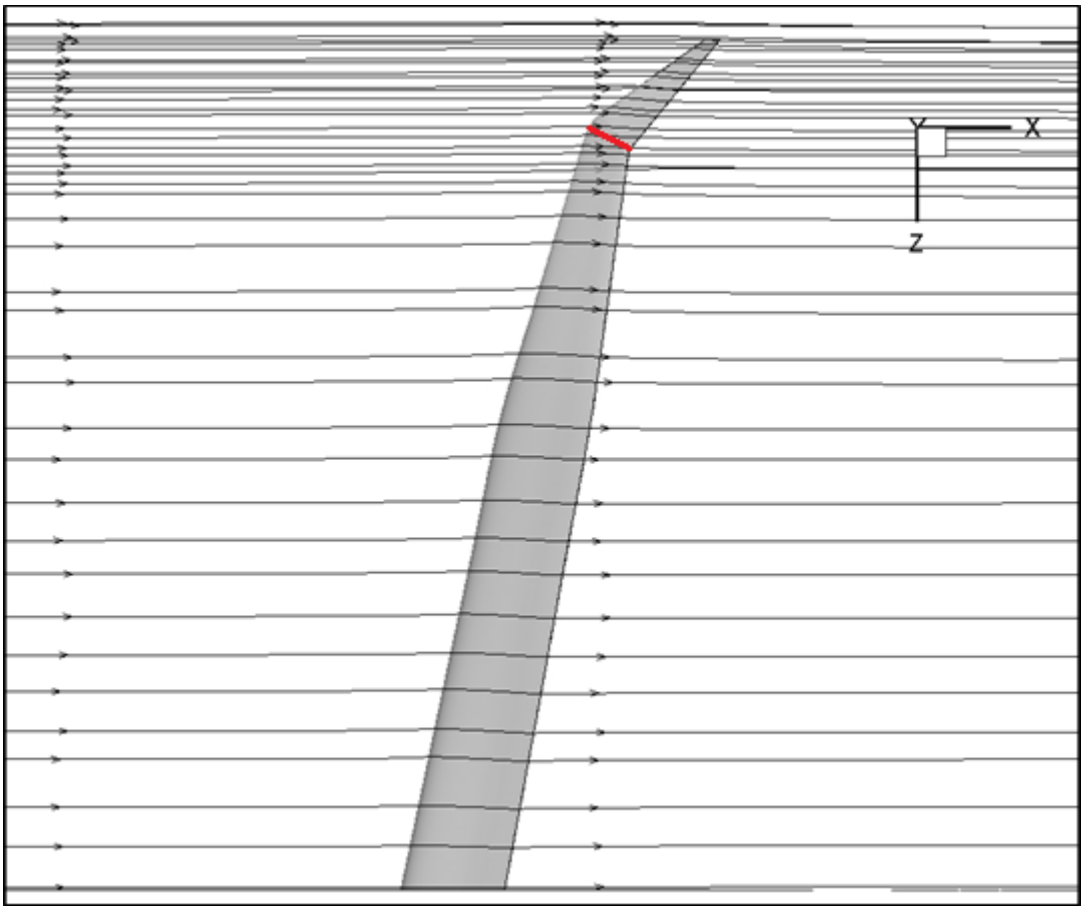

Figure 26 – Fluent Prediction of Streamlines Over Step for Fully-Swept VGRWT/NCE Tip (Step drawn in red)

Hoerner indicated that the drag coefficient over a surface imperfection can be given by:

$$C_D = 4 * c_D * \sqrt[3]{\frac{h}{x}} \tag{7}$$

In this instance, x is the distance from the leading edge to the imperfection, h is the height of the imperfection, and c_D is referred to as an independent coefficient that varies with the shape of the imperfection. For this study, the independent coefficient was taken to be $c_D = 0.16$, which corresponds to a rounded step [Ref. 16, Ch. 5, Fig. 10]. The height of the step was taken to be comparable to standard skin thickness, in this case between one and three tenths of an inch. Finally, the distance to the joint was taken to be mid-chord, approximately 30 in. These results

are presented assuming the joint is in crosswise flow. However, with the joint nearly normal to the wing leading edge, this is not true for the current case. Hoerner also presents a method to transition between crosswise and longitudinal flow with respect to a step, given by Equation 8:

$$C_D = \sin^2 \beta \tag{8}$$

where β is the angle of the joint, 16° in this case. Therefore, Equations 7 and 8 combine to form the final relation:

$$C_{D_{step}} = \left(4 * c_D * \sqrt[3]{\frac{h}{x}} \right) * \sin^2 \beta \tag{9}$$

Using this result and the results of the viscous drag estimation from Section 3.2.3, we can estimate the influence of the step on the drag of the VGRWT/NCE tip in the following way:

$$\frac{D_{step}}{D_{tip}} = \frac{2 * h * c * C_{D_{step}}}{C_{D_{tip}} * S_{tip}} \tag{10}$$

For this analysis, the area of the tip, S_{tip}, was held constant at 50 ft^2 , while the drag coefficient on the tip was also held constant at 0.0082, from the results presented in Table 8 for the fully-swept VGRWT/NCE tip. The chord, *c*, was taken to be 60 inches, which is the approximate value of the chord at the VGRWT/NCE tip joint. The results are presented as Table 9. As expected, the drag coefficient is very dependent on the height of the step. Indeed, the maximum skin thickness contributes 0.5% more drag to the tip than the smallest step height. Though this seems small, any increase in drag will negatively impact fuel efficiency, therefore, with a common minimum skin thickness of 0.08 in, it is not unrealistic to design the height of the step as close to this minimum value as possible. It is also important to insure the step angle from Equation 8 is kept as small as possible. In the worst case scenario of a crosswise step, the drag

would increase to nearly 15 times the values presented. Overall, the joint contributes a small, but not insignificant portion of the drag coefficient for the VGRWT/NCE tip.

Table 9 – Drag Due to Wing/VGRWT/NCE Joint

Step Height h, in	$C_{D_{step}}$	**Percent of Drag on VGRWT/NCE Tip Due to Step**
0.1	0.0073	0.14 %
0.15	0.0083	0.25 %
0.2	0.0092	0.37 %
0.25	0.0098	0.50 %
0.3	0.0105	0.64 %

It should be noted that the above results assume a perfectly sealed joint. However, the results would change significantly if there is an open gap between the wing and tip. Hoerner demonstrates that for a perfect sharp-edged joint, the independent coefficient is 0.4. However, if there is a gap as little as 3 mm between layers, this coefficient increases to 0.6 when the gap faces the flow [16]. Though it is not anticipated that the joint will face the freestream, reverse flow into the joint would still contribute to an increase in drag, turbulence and noise. Therefore, care should be taken to ensure that the joint is as solid as possible. This will most likely involve sealing the joint with flexible skin or a rubber fairing.

Although reverse flow into an open joint is not anticipated, a large pressure difference could cause substantial airflow, as the pressure inside the airfoil attempts to equalize with the pressure outside the airfoil. Therefore, pressure contours were taken from the *Fluent* results for

the unswept VGRWT/NCE tip and the fully-swept VGRWT/NCE tip. The contours shown are at the main wing/VGRWT/NCE junction and are presented as Figure 27. At cruise altitude, the ambient pressure is approximately 2.25 psi. This is nearly identical to the pressure produced by the underside of the wing. However, the pressure above the wing is slightly lower, at approximately 1.45 psi. Therefore, some equalizing flow will be present. This leakage flow could also be minimized with the implementation of the aforementioned flexible skin or rubber strips.

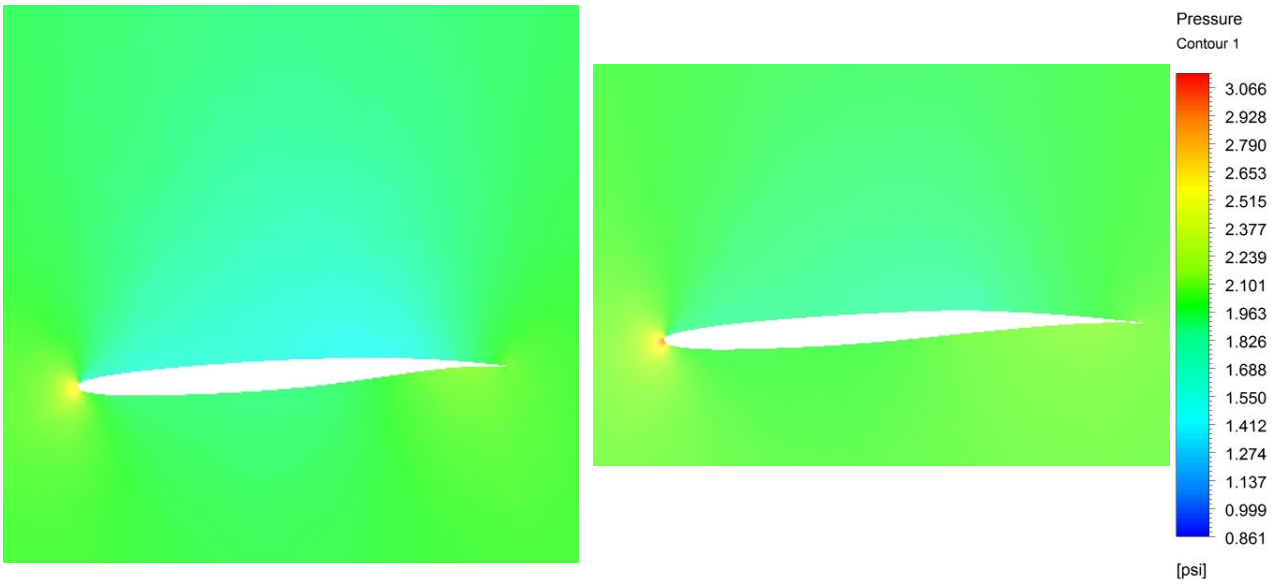

Figure 27 – Fluent Prediction of Pressure Contours of Unswept (Left) and Fully-Swept (Right) VGRWT/NCE Wingtip at Main Wing/Wingtip Junction

Chapter 4: Conclusions

Previous applications of wingtip treatments have shown that tangible gains can be made with regard to drag reduction and fuel burn. However, these treatments, be they blended winglets or raked wingtips, are rarely optimized for all phases of flight. Generally a compromise is made to improve performance at cruise conditions, to the detriment of take-off and landing characteristics. With this in mind, a study was conducted analyzing the performance of a variable geometry raked wingtip applied to a baseline SUGAR TBW design. The VGRWT/NCE tip will be unswept for low-speed flight stages and swept for cruise conditions. We have shown that the VGRWT/NCE tip provides noticeable aerodynamic performance increases over an unmodified wingtip.

Preliminary analysis focused on the effect that the VGRWT/NCE has on the entire wing system. The VLM code, *Tornado*, analysis showed that the lift would increase, with a subsequent decrease in drag as a result of the new wingtip. Closer examination revealed that the unswept VGRWT/NCE tip provided more lift than the baseline wing tip and the swept VGRWT/NCE tip. This result justifies having the VGRWT/NCE tip unswept during take-off and landing, when lift is at a premium. Also, the swept configuration presented a lower drag coefficient than the baseline SUGAR wingtip, which validates the concept of a swept wingtip for cruise. The pitching moment of the wing would also increase, leading to a more stable platform. Inviscid CFD simulations run through *ANSYS Fluent* largely corroborated these results, with a difference in incidence angle of approximately one-tenth of a degree and a consistent 9% difference in pitching moment between methods. The excellent agreement between methods confirms that VLM analysis, if conducted carefully, is a viable alternative to the often complicated and time consuming CFD simulations.

Thorough analysis was also conducted on the performance of the wingtips alone. This analysis showed that the lift performance of the unswept VGRWT/NCE tip and the baseline SUGAR tip was nearly identical, as designed. It also showed that the swept tip configurations produced increasingly smaller amounts of lift as the sweep angle increased. This was also expected as the sweep results in a smaller aspect ratio. The moments produced by the VGRWT/NCE tips provided unexpected results. It was found that the three-quarter sweep configuration produces the largest moment, while the one-quarter sweep model produces moments closest to the baseline SUGAR tip. Since the largest moment was produced with the three-quarter sweep tip, it could be argued that increasing the wingtip sweep beyond this configuration would result in only small gains in performance. Also, the large moments produced on the VGRWT/NCE tip can be used with a flexible wing for roll control or gust load alleviation. Due to the fact that the largest moments occur at the three-quarter sweep position, the actuator needed to move the VGRWT/NCE tip could be smaller than originally anticipated. Therefore, decreasing the maximum sweep may also result in the added benefit of reducing the cost, complexity, and weight of the swing mechanism itself.

Finally, a small study was performed on the effect of the step at the joint of the main wing and the VGRWT/NCE tip. This analysis revealed that the step would cause small additional drag, though careful design would minimize its impact.

The effect of the VGRWT/NCE tip on the SUGAR wing observed through this study is substantial. With these results in mind, the VGRWT/NCE tip is a viable option for the tip treatment of a next generation airliner. The VGRWT/NCE tip allows the wing to be optimized for all phases of flight and with fuel efficiency becoming an increasingly large design driver, even a small performance gain has the potential to be significant.

References

[1] Stephenson, D. "Envisioning Tomorrow's Aircraft." The Boeing Company, 16 August 2010. Web. < http://www.boeing.com/Features/2010/06/corp_envision_06_14_10.html>.

[2] Gur, O., Schetz, J.A., Mason, W.H. "Aerodynamic Considerations in the Design of Truss-Braced Wing Aircraft," AIAA Paper 2010-4813, *28th AIAA Applied Aerodynamics Conference*, June 28 – July 1, 2010, Chicago, Illinois.

[3] de Mattos, B., Macedo, A., da Silva Filho, D. "Considerations about Winglet Design," AIAA Paper 2003-3502, *21st Applied Aerodynamics Conference*, June 23-26, 2003, Orlando, Florida.

[4] Halpert, J., Prescott, D., Yechout, T., Arndt, M. "Aerodynamic Optimization and Evaluation of KC-135R Winglets, Raked Wingtips, and a Wingspan Extension," AIAA Paper 2010-57, *48th AIAA Aerospace Sciences Meeting Including the New Horizons Forum and Aerospace Exposition*, January 4-7, 2010, Orlando, Florida.

[5] Spearman, M. L. "Aerodynamic Research at NACA/NASA Langley Related to the Use of Variable-Sweep Wings," AIAA Paper 2012-0956, *50th AIAA Aerospace Sciences Meeting including the New Horizons Forum and Aerospace Exposition*, January 9-12, 2012, Nashville, Tennessee.

[6] Kress, R. "Variable Sweep Wing Design," AIAA Paper 83-1051, Archive Set 237: Generic Session, January 1, 1963.

[7] Bertin, J. *Aerodynamics for Engineers*. 4th ed. Upper Saddle River, NJ: Prentice Hall, 2002. pp. 260-78.

[8] Melin, T. *A Vortex Lattice MATLAB Implementation for Linear Aerodynamic Wing Applications*. MS Thesis. Royal Institute of Technology, Stockholm, 2000. Web. <http://www.redhammer.se/*Tornado*/thesis.pdf>.

[9] Melin, T. *User's Manual, Reference Guide Tornado 1.0*. Royal Institute of Technology, Stockholm, 2000. Web. <http://www.redhammer.se/*Tornado*/manual.pdf>.

[10] Welsted, J., Reitz, B., Crouse, G. "Modeling Fuselage Aerodynamic Effects in Aircraft Design Optimization," AIAA Paper 2012-0394, *50th AIAA Aerospace Sciences Meeting including the New Horizons Forum and Aerospace Exposition*, January 9-12, 2012, Nashville, Tennessee.

[11] Melin, T., Isikveren, A. Friswell, M., "Induced-Drag Compressibility Correction for Three-Dimensional Vortex-Lattice Methods," *Journal of Aircraft*, Vol. 47, No. 4, 2010, pp. 1458 – 1460.

[12] "UIUC Airfoil Coordinates Database." *UIUC Airfoil Data Site*. University of Illinois at Urbana-Champaign, Web. <http://www.ae.illinois.edu/m-selig/ads/coord_database.html>

[13] Hays, A. "12.6 Drag Due to Lift (Induced Drag)." ADAC, 28 March 2009. Web. <http://www.adac.aero/linked/12.6_drag_due_to_lift.pdf >.

[14] Raymer, D. *Aircraft Design: A Conceptual Approach.* 4th ed. Reston, VA: American Institute of Aeronautics and Astronautics, 2006. pp. 347-348.

[15] White, F. *Viscous Fluid Flow.* 3rd ed. New York, NY: McGraw-Hill Higher Education, 2006. pp. 314-315.

[16] Hoerner, S. *Fluid-dynamic Drag: Practical Information on Aerodynamic Drag and Hydrodynamic Resistance*. Midland Park, N.J: Dr.-Ing. S.F. Hoerner, 1958. pp. 5-6 – 5-9.